HAL
open science

Hybrid Quantum Circuits

Audrey Cottet

To cite this version:

Audrey Cottet. Hybrid Quantum Circuits. Condensed Matter [cond-mat]. Ecole normale supérieure - ENS PARIS, 2017. tel-01536225

HAL Id: tel-01536225

https://hal.science/tel-01536225v1

Submitted on 10 Jun 2017

HAL is a multi-disciplinary open access archive for the deposit and dissemination of scientific research documents, whether they are published or not. The documents may come from teaching and research institutions in France or abroad, or from public or private research centers.

L'archive ouverte pluridisciplinaire **HAL**, est destinée au dépôt et à la diffusion de documents scientifiques de niveau recherche, publiés ou non, émanant des établissements d'enseignement et de recherche français ou étrangers, des laboratoires publics ou privés.

Thesis for the Research Direction Habilitation from the ENS-Paris

Hybrid Quantum Circuits

Audrey Cottet

Delivered on May 30th 2017 on the recommendation of:

Guido Burkard

Milena Grifoni

Thierry Martin

Jean-Michel Raimond

Pascale Senellart

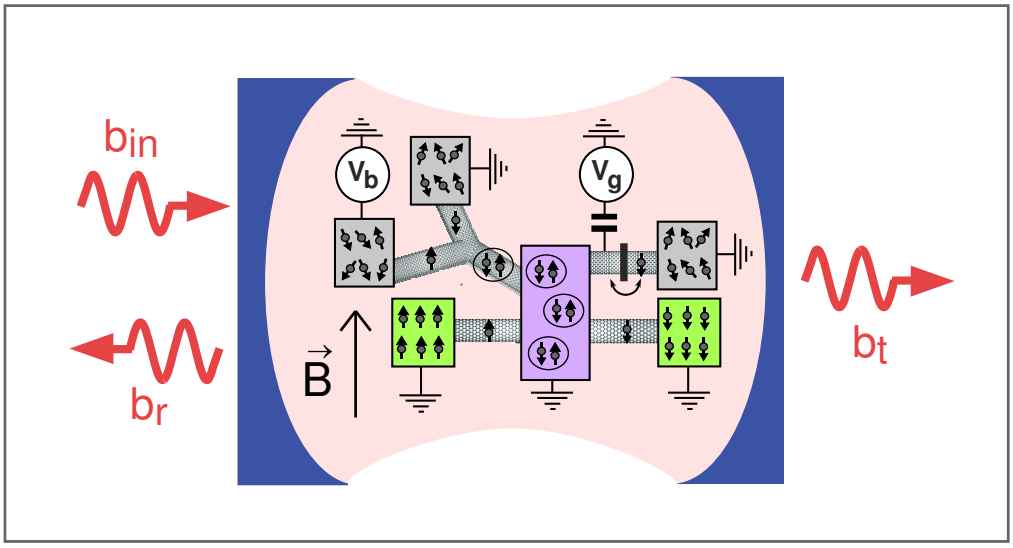

Remerciements/Acknowledgements

J'aimerais tout d'abord remercier Takis Kontos pour la collaboration scientifique très fructueuse que nous avons commencée en 2005 à Bâle et qui est devenue de plus en plus intense avec les années. C'est pour moi une grande chance d'avoir un partenaire aussi formidable (dans tous les domaines de la vie!). J'ai également la chance de travailler sur les aspects théoriques avec Benoit Douçot, dont la vision très personnelle de la physique est toujours extrêmement enrichissante. Je suis très heureuse de remercier tous les membres passés et présents du groupe HQC: Laure Bruhat, Lauriane Contamin, Dora Crisan, Tino Cubaynes, Subhadeep Datta, Matthieu Delbecq, Matthieu Desjardins, Matthieu Dartiailh, Zaki Legthas, François Mallet, Federico Valmora, et Jérémie Viennot. C'est un rêve pour un(e) théoricien(ne) de la physique mésoscopique d'avoir une collaboration privilégiée avec une équipe expérimentale si dynamique et talentueuse. Un grand merci à André Thiaville et Stanislas Rohart pour leur aide précieuse sur les questions de micromagnétisme, indispensable à la réussite de certaines expériences phares du groupe HQC. J'aimerais remercier le laboratoire Pierre Aigrain dans son ensemble, et en particulier les services techniques et administratifs (Yann Colin, Anne Matignon, Olga Hodges, ...) pour leur soutien logistique, et les directeurs successifs (Claude Delalande, Jean-Marc Berroir, et Jérôme Tignon) pour leurs conseils avisés. Merci aux responsables du groupe théorie, Gérald Bastard et Nicolas Regnault pour leur bienveillance. Je suis reconnaissante envers mes collègues de thèse et de post-doc, le groupe Quantronique ainsi que Christophe Bruder et Wolgang Belzig, pour avoir contribué à ma formation scientifique. Un grand merci à Guido Burkard, Milena Grifoni, Thierry Martin, Jean-Michel Raimond, et Pascale Senellart d'avoir bien voulu être membres de mon jury de HDR. Enfin, merci à mes parents Françoise et André pour leur aide précieuse dans toutes sortes de circonstances, même les plus acrobatiques. Et merci à mon fils Alban de s'accommoder d'une maman un peu dans la lune...

The HQC group in 2017. Top row, from left to right: Tino Cubaynes, Federico Valmora, Raphael Lescanne, Matthieu Dartiailh, Audrey Cottet. Bottom row, from left to right: Matthieu Desjardins, Lauriane Contamin, Takis Kontos, Franois Mallet and Zaki Legthas

CONTENTS

1. Introduction 3

1.1 Scientific profile 3

1.2 Research highlights 4

1.3 Outline of the report 6

2. Early research results 7

2.1 Implementation of a quantum bit in a superconducting circuit (PhD thesis) 7

2.2 Current noise and spin-dependent transport in nanocircuits (post-docs) 8

2.2.1 Positive current cross-correlations in a quantum dot circuit . . . 8

2.2.2 Electronic transport in mesoscopic circuits with spin-active interfaces 9

3. Superconducting/ferromagnetic hybrid circuits 13

3.1 Introduction 13

3.2 Spin-dependent boundary conditions for diffusive hybrid circuits 13

3.3 Triplet superconducting correlations in a normal metal 15

4. Gate controlled nanospintronics 17

4.1 Introduction 17

4.2 Multiterminal circuits 17

4.3 Gate-modulated spin-precession 18

5. Cavity QED with hybrid nanocircuits 21

5.1 Introduction 21

5.2 Physical implementation of the nanocircuit-photon coupling 22

5.3 Theoretical description of the nanocircuit-photon coupling 23

5.3.1 Comparison between the different types of cavity QED experiments 23

5.3.2 Minimal coupling Hamiltonian 24

5.3.3 Photonic pseudo-potential picture 25

5.4 Anderson-like Hamiltonian for Mesoscopic QED 27
5.5 Theoretical description of the cavity signals in the semiclassical linear limit 27
5.6 Double quantum dot with normal metal reservoirs 29
5.7 Coherent coupling between a single spin and cavity photons 33
5.8 Single quantum dot contacted to fermionic reservoirs 36
5.9 Majorana nanocircuits 38
5.10 The Cooper pair splitter 41

6. Conclusion and perspectives 43

1. INTRODUCTION

1.1 Scientific profile

Nanoscale electronic circuits placed at low temperatures exhibit quantum effects which are the basis of quantum electronics. My research takes its roots in this field, which has connections with quantum information, strongly correlated systems, topological matter and Cavity QED. Before describing my scientific achievements in this vast landscape, it can be useful to describe briefly my career and scientific approach. I first did an experimental thesis on Josephson superconducting circuits in the Quantronics group of Saclay (1999-2002). Then, I did a technical retraining during six years of post-doctoral studies (Basel (2002-2005), Orsay (2005-2007), Jussieu (2007–2008)) in order to become a condensed matter theorist. During these years, I studied the theory of quantum dot circuits and superconducting/ferromagnetic hybrid structures. In October 2008, I was hired as a CNRS researcher in the Theory Group of Laboratoire Pierre Aigrain (LPA) at the Ecole Normale Supérieure de Paris. Since then, I use my double education as a theorist and as an experimentalist to perform theoretical works on Hybrid Nanocircuits in strong connection with experimental researchers. I devote a significant part of my time to a close collaboration with the experimental team Hybrid Quantum Circuits (HQC) of Takis Kontos at the LPA. I am a co-director for several Phd theses in this group. I follow closely the analysis and interpretation of the experimental data, as well as the promotion of the results. I also participate to the choices for the future experiments of this team. I sometimes work with other experimental groups. For instance, in 2016, I have participated to the theoretical interpretation of data from the group of E. Laird in Oxford. In parallel, I also work upstream of experiments, in order to push further the fundamental understanding of hybrid nanostructures, as well as to predict new effects and propose new experiments. In this framework, I have established a close collaboration with the Laboratoire de Physique Théorique of University Paris VI (B. Douçot). I also regularly collaborate with theory teams outside France (England, Germany, Norway, Nederlands and Spain).

1.2 Research highlights

Today, one of the most popular research goal in physics is the development of a quantum computer, which would exploit quantum parallelism to perform tasks intractable with nowadays' computers. This requires first to build the basic unit of a quantum computer, or quantum bit, which is a controllable quantum two level system. Superconducting microcircuits are very interesting in this context, because the rigidity of the superconducting phase strongly reduces their accessible space of states. Along this direction, my experimental PhD on Josephson circuits enabled the first realization of a superconducting quantum bit with a coherence time of the order of a microsecond [*Vion et al, Science 2002*]. During my post-docs, I moved to the field of quantum transport and considered nanocircuits with a greater microscopic complexity, due to the presence of non-superconducting elements, such as ferromagnetic electrodes. This gives an access to the electronic spin degree of freedom, which could represent another interesting possibility to encode quantum information, due to the potentially long coherence time of spins in nanostructures. I studied current noise and spin-dependent transport in quantum dots with ferromagnetic contacts [*Cottet et al, Phys. Rev. Lett 2004*] and superconductor/ferromagnet hybrid circuits [*Cottet et al, Phys. Rev. Lett 2008*]. This led me to collaborate with the experimental team of C. Schönenberger in Basel, for the realization of the first spin transistor [*Sahoo et al., Nature Physics 2005*] which would be the simplest component of a gate-controlled nanospintronics.

Since my arrival at ENS-Paris, my research activity has focused on hybrid quantum circuits. The combination of conductors with different dimensionalities or electronic orders produces a wealth of new phenomena and functionalities. I have explored three different possibilities along this direction. I have first pushed further the study of purely metallic superconducting/ferromagnetic hybrid structures, which I began in Basel. These devices enable one to obtain non-conventional superconducting correlations, which present a fundamental interest but also a technical interest due to the realization of new functionalities in superconducting circuits. I have collaborated with Y. Nazarov (Delft) and W. Belzig (Constance) to establish a new framework for the description of the interfaces between superconducting and ferromagnetic materials in the diffusive regime [*Cottet et al., Phys. Rev. B 2009*]. This fills a technical gap which was raising problems since several years for the description of hybrid structures. Using these boundary conditions, I have proposed a geometry which could facilitate the study of exotic superconducting correlations corresponding to Cooper pairs in a triplet with

spin 1 state [*Cottet, Phys. Rev. Lett. 2011*].

I have also pursued my work on gate-controlled nanospintronics. The use of phase-coherent nanoconductors, such as carbon nanotubes at low temperatures, enables one to control electronic transport with electrostatic gates, thanks to quantum interference effects. Hence, the combination of nanoconductors and ferromagnetic contacts leads to many new spintronics functionnalities, based on the electric control of the spin degree of freedom. I have considered new concepts not investigated with the spin transistor developed in Basel, which was based on a carbon nanotube with two ferromagnetic contacts magnetized in colinear directions. For instance, I have predicted a non-local spin transistor effect, in a coherent nanoconductor with four contacts [Cottet et al., Phys. Rev. B 2009]. I have collaborated with the HQC group on the corresponding experiment [*Feuillet-Palma et al., PRB 2010*]. I have also collaborated to the observation of a gate-controlled spin-precession effect in a biased-voltage quantum dot with two ferromagnetic contacts magnetized in non-colinear directions [*Crisan et al, Nature Communications 2016*].

Finally, I have now an intense activity on Cavity Quantum Electrodynamics (QED) with hybrid nanocircuits, in close collaboration with the HQC group. Cavity QED experiments which couple cavity photons to two level systems such as two level atoms or superconducting quantum bits enable a fundamental study of the light-matter interaction as well as the development of powerful quantum computing architectures. It can be interesting to push further the light/matter hybridization by coupling cavity photons to more complex hybrid nanocircuits. This represents a qualitatively new way to investigate the electronic behavior of these nanocircuits. I have thus collaborated to the first experiment reporting an observation of a single quantum dot circuit through a microwave cavity [*M.R. Delbecq, Phys. Rev. Lett. 2011*]. I have established a general Hamiltonian to describe this class of experiment [*Cottet et al., Phys. Rev. B 2015*]. I have pointed out that in the semiclassical limit, the microwave cavity can directly measure the charge susceptibility of a nanocircuit, which can be affected by tunneling to fermionic reservoirs [*Cottet et al., Rapid. Comm. 2011*]. This has been confirmed thanks to the detailed interpretation of experimental data, which I have performed in collaboration with the HQC group [*Bruhat et al, Phys. Rev. X 2016*]. The use of hybrid circuits in the context of Cavity QED gives a photonic access to new degrees of freedom, such as the electronic spin degree of freedom. For instance, one could obtain a strong coupling between a single spin trapped in a double quantum dot and cav-

ity photons, thanks to ferromagnetic contacts, [*Cottet and Kontos, Phys. Rev. Lett. 2010*]. I have collaborated to the first experimental realization of this device [*Viennot et al., Science 2015*]. I have also proposed different experiments which would exploit the nanocircuit/photon coupling in order to probe non-trivial electronic states in a nanocircuit. For instance, I have proposed to use a microwave cavity to characterize exotic condensed matter states such as split Cooper pairs [*Cottet et al, Phys. Rev. Lett. 2012*] or Majorana bound states [*Dartiailh et al., Phys. Rev. Lett. 2017, in press*]. The experiments corresponding to these proposals are under development in the HQC group, with my close support. Along the same direction, I have participated to the recent observation of the freezing of charge dynamics in a Kondo dot, thanks to a microwave cavity [*Desjardin et al., Nature 2017*].

1.3 Outline of the report

In chapter I, I summarize briefly my Phd thesis and my post-doc results. In the next three chapters, I summarize the results that I have obtained at the LPA by dividing them into three themes: superconducting/ferromagnetic hybrid structures, gate-controlled nanospintronics, and Cavity QED with hybrid nanocircuits. I will discuss in more details this last activity which is the most recent. I will finally present a conclusion and perspectives.

2. EARLY RESEARCH RESULTS

2.1 Implementation of a quantum bit in a superconducting circuit (PhD thesis)

Superconducting microcircuits are interesting systems in the context of quantum information science because, due to the rigidity of the superconducting phase, they can be used to build reliably devices with a few accessible quantum states. For instance, the Cooper pair box is a submicronic superconducting island, contacted to a superconducting reservoir through a Josephson junction. To describe the quantum state of this circuit, it is sufficient to use the number $\hat{n}$ of Cooper pairs in the island. Besides, if Coulomb interactions in the island are sufficiently strong, only a few values of $\hat{n}$ are accessible in practice. The purpose of my thesis, performed in the Quantronics group (CEA-Saclay), from 1999 to 2002, was to realize a prototype for the quantum bit, out of a Cooper pair box. More precisely, I had to build the two states $|0\rangle$ and $|1\rangle$ of the quantum bit out of a few charge states of the superconducting island in the Cooper pair box. For that purpose, I performed a theoretical evaluation of decoherence ef-

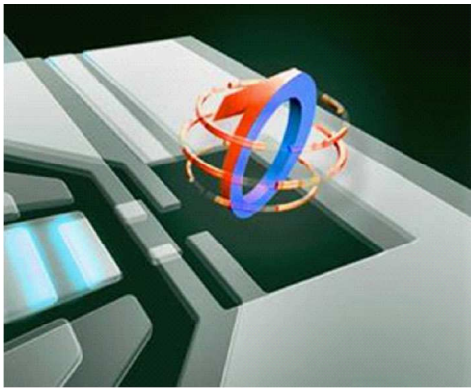

Fig. 2.1: Artist view of the Quantronium circuit

fects in the Cooper pair box, in order to design a circuit with a long enough coherence time[1, 2, 3]. Meanwhile, I tested experimentally several readout strategies for the state of the Cooper pair box, based on charge or current measurements[1, 2, 3]. The most promising circuit, the Quantronium, was proposed theoretically in Ref.[3]. The first

experimental realization of this circuit showed coherent oscillations between the states $|0\rangle$ and $|1\rangle$ during a time of 0.5 microseconds[4]. This coherence time was sufficient to envision the development of a quantum processor. Hence, my thesis encouraged the development of other types of quantum bits. An important concept introduced in the framework of this thesis is the concept of "sweet spot" for charge noise[3]. The transition frequency ω_{01} of the Quantronium depends on the gate voltage V_g of its superconducting island. However, charge fluctuators in the vicinity of the island induce fluctuactions of V_g. As a result ω_{01} fluctuates, which causes decoherence of the Quantronium state. This effect can be significantly minimized by operating the device at its sweet spot where $\partial\omega_{01}/\partial V_g = 0$. Later, this concept was used in other single electron devices such as the singlet-triplet spin quantum bit in a double quantum dot[6]. Thanks to this thesis, I could learn the experimental techniques of e-beam nanolithography, metallic evaporation, cryogenics, low-noise measurements and radiofrequencies. I could also learn the theoretical description of quantum superconducting circuits.

2.2 Current noise and spin-dependent transport in nanocircuits (post-docs)

Spin transport is widely exploited in industrial spintronics devices based on ferromagnetic materials[5]. By extension, it is very interesting to investigate the possibilities offered by the spin degree of freedom in quantum electronics. For my theoretical retraining, I thus studied mainly current noise and spin-dependent transport in quantum dots and quantum point contacts.

2.2.1 Positive current cross-correlations in a quantum dot circuit

I considered the problem of the sign of cross-correlations between the electrical currents in different branches of an electronic nanocircuit. A similar quantity had been thoroughly investigated in quantum optics to characterize photon sources[7]. In this case, it is more easy to obtain positive cross-correlations due to the bosonic nature of photons. In contrast, negative cross-correlations were expected for electronic currents, due to the fermionic nature of electrons[8, 9, 10]. I first studied the case of a quantum dot with a single electronic orbital, contacted to three fermionic reservoirs, by using a master equation description[11]. Surprisingly, I found that if the reservoirs are ferromagnetic, Coulomb interactions in the dot can produce positive current cross-correlations. This

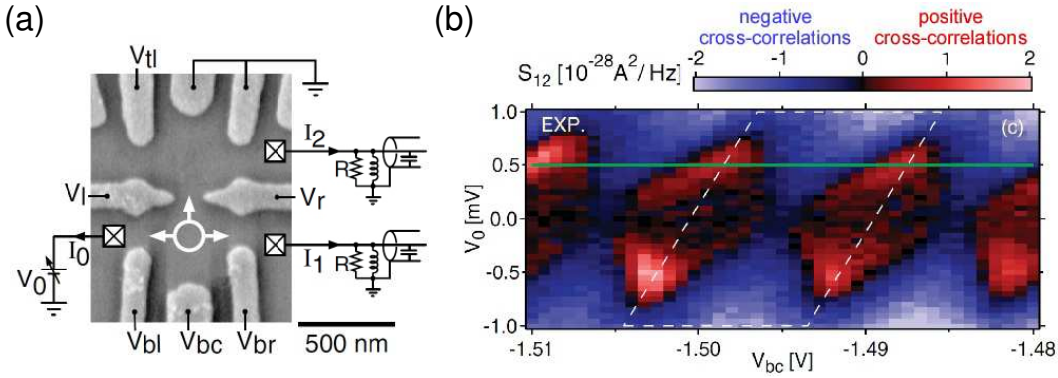

Fig. 2.2: Observation of positive cross-correlations in a semiconducting quantum dot circuit with three terminals, taken from Y. Zhang et al, Phys. Rev. Lett. 2007. (a) Picture of the sample (b) Cross correlations S_{12} between the currents I_1 and I_2 versus the gate voltage V_{bc} and the bias voltage V_0. The red and blue shades correspond to positive and negative cross-correlations respectively. Positive cross-correlations are obtained in the Coulomb blockade areas, where V_0 is too small to overcome interaction effects in the dot.

is due to the fact that the electrons can tunnel through the circuit only in short time windows where the dot is not blocked by a minority spin. This "dynamical channel blockade" leads to a bunching of tunneling events through the dot. This effect can also be obtained without lifting spin-degeneracy if a quantum dot with two orbital levels is used, provided the two orbitals have different couplings to the fermionic reservoirs[12]. This last possibility was realized experimentally in the group of Charles Marcus in Harvard[13], as illustrated by Fig. 2.2.

2.2.2 Electronic transport in mesoscopic circuits with spin-active interfaces

I pointed out in several works the importance of the concept of spin-dependent scattering phases at the interface between a ferromagnetic material and a non-magnetic material (or SDIPS, for "Spin-Dependence of Interfacial Phase Shifts"). I showed that the SDIPS can modify significantly the behavior of many different types of hybrid circuits. For instance, it can induce an effective Zeeman field in a diffusive superconducting layer tunnel-contacted to a ferromagnet[14]. It can also dephase the spatial oscillations of superconducting correlations which propagate in a diffusive ferromagnet tunnel-contacted to a superconductor[15]. This last result enabled a quantitative interpretation of several pioneering experiments in this field[18, 19], which were not fully understood formerly. For this study, I used the quasiclassical theory of superconductivity (Eilenberger equations and Usadel equations).

I also studied the effects of the SDIPS on superconducting/ferromagnetic quantum point contacts, by using the Landauer-Büttiker scattering approach. I showed that the SDIPS can produce unusual subgap resonances or an apparent gap reduction in the conductance of these contacts[20]. This was questioning the interpretation of such measurements. I showed that in this context, noise measurement could be useful[21].

Finally, superconductivity is not a necessary ingredient to observe physical consequences of the SDIPS. Indeed, the SDIPS can also cause an effective Zeeman field in a coherent nanoconductor. Figure 2.3 represents a quantum dot made out of a portion with length ℓ of a single-channel nanoconductor, delimited by two ferromagnetic contacts. I first considered this situation in a non-interacting scattering picture. The phase

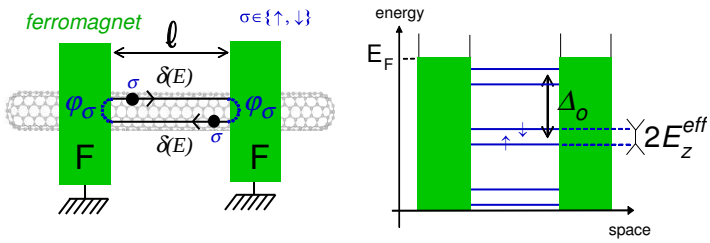

Fig. 2.3: (a) Quantum dot formed by a portion with length ℓ of nanoconductor (here a carbon nanotube) delimited by two ferromagnetic reservoirs (in green). The dot levels have an effective Zeeman spin splitting $2E_z^{eff} = (\varphi_\uparrow - \varphi_\downarrow)\,\hbar v_F/\ell$ because electrons with spin σ have a spin dependent reflection phase φ_σ on the ferromagnetic reservoirs. The separation between the different spin pairs of orbital levels is $\Delta_o = \pi\hbar v_F/\ell$

shift acquired by an electron which crosses once the dot is $\delta(E) = \ell(k_F + (E - E_F)/v_F)$, where E_F, k_F and v_F are the Fermi energy, wavevector and velocity inside the nanoconductor and E is the electron energy treated at first order. The electron can be reflected on the ferromagnetic contacts with spin-dependent reflection phases φ_σ with $\sigma \in \{\uparrow, \downarrow\}$, because the Stoner exchange fields inside the ferromagnets provide a spin-dependent confinement potential for electrons in the dot. Hence, the dot orbital energies are given by the resonant condition

$$2\delta(E) + 2\varphi_\sigma = 2\pi n \tag{2.1}$$

with $n \in \mathbb{N}$ (see Fig.2.3a). As a result, the dot orbitals are subject to an effective Zeeman spin splitting[22]

$$2E_z^{eff} = (\varphi_\uparrow - \varphi_\downarrow)\,\hbar v_F/\ell \tag{2.2}$$

The effective Zeeman field of Eq.(2.2) scales with ℓ^{-1} because it is an interference effect between the two contacts. Due to this factor, E_z^{eff} can reach values of the order of

several Teslas for short quantum dots. This value is much larger than stray fields from standard ferromagnets, which are independent of ℓ and reach typically a few 100 mT. Furthermore, the effective field of Eq.(2.2) presents the advantage of being local, which can be useful for building complex devices, as we will see later. Note that from Eq.(2.1), the energy separation between the different spin doublets is

$$\Delta_o = \pi\hbar v_F/\ell \tag{2.3}$$

In a second step, I studied the case of a quantum dot with Coulomb blockade contacted to ferromagnetic contacts[23], thanks to a technique which consists in truncating the equations of motions for the dot Green's functions, following Ref.[24]. I used this approach to interpret data obtained in the group of C. Schönenberger in Basel, for a spin valve based on a carbon nanotube with two ferromagnetic contacts[25]. A spin-valve is characterized by its magnetoresistance, which is the difference between its conductance for ferromagnetic contacts magnetized in parallel and antiparallel directions. The giant magnetoresistance obtained in this experiment suggests the existence of a contact-induced effective Zeeman field of the order of 2 tesla. Due to this field, a local spin transistor was obtained. In other worlds, the magnetoresistance of the quantum dot could be controlled with the gate voltage of the dot. Note that in the interacting case, contact-induced effective field effects were also investigated with other Hamiltonian techniques[26, 27, 28, 29]. Effective fields will be at the heart of a later discuss in this report on the spin/photon coupling in hybrid quantum dot circuits (section 5.7)

3. SUPERCONDUCTING/FERROMAGNETIC HYBRID CIRCUITS

3.1 Introduction

Can two antagonistic electronic orders coexist in a hybrid structure? This problem is epitomized by superconducting/ferromagnetic hybrid circuits. A conventional BCS superconductor hosts Cooper pairs made out of two electrons in a spin singlet state. In contrast, a ferromagnet tends to favors the alignment of spins along its magnetization vector. However, superconducting and ferromagnetic correlations can coexist in a superconductor/ferromagnet bilayer, due to a modification in the nature of these correlations[16]. Indeed, triplet correlations between opposite spins (triplet with spin 0) or between equal spins (triplet with spin 1) can appear in the hybrid structure. These correlations are cousins of those predicted in the bulk FFLO state[17], or of those expected in some exotic compounds like SrRuO4. The production and control of such correlations in artificial nanostructures has thus a fundamental interest. This can also have a technical interest. For instance, triplet correlations with spin 0 enable one to obtain π Josephson junctions which produce permanent currents in a superconducting loop, in the absence of any external magnetic field. Such π Josephson junctions could therefore be interesting components to build new Josephson circuits.

3.2 Spin-dependent boundary conditions for diffusive hybrid circuits

The spatial propagation of superconducting correlations in a metal with diffusion impurities can be described with the Usadel equation[30]

$$\hbar D \overrightarrow{\nabla}_{\vec{r}} \left(\check{G}(\vec{r}) \overrightarrow{\nabla}_{\vec{r}} \check{G}(\vec{r}) \right) = -i\varepsilon[\tau_3, \check{G}(\vec{r})] \tag{3.1}$$

The Usadel equation is a diffusion equation for the isotropic Green's function $\check{G}(\vec{r})$ which characterizes superconducting correlations at coordinate $\vec{r}$. Above, I give this equation for the case of a normal metal, for simplicity. I note D the diffusion constant of the metal, and ε the quasiparticle energy. From the Usadel equation, inside each material m, the superconducting correlations evolve on a scale which I will note ξ_m. The

Usadel equation can be derived by using approximations suitable for the diffusive limit where electrons are scattered by diffusion impurities. However, the Usadel equations are not sufficient to describe the behavior of a hybrid structure, because one also needs to describe the interfaces between the different materials. This task can be done by using boundary conditions which relate the values $\check{G}_L$ and $\check{G}_R$ of $\check{G}(\vec{r})$ at the two sides of the interface. These boundary conditions are not trivial to obtain because on the scale of the interface, the approximations performed to obtain the Usadel equations are not valid. This is why, until recently, the only available boundary conditions where spin-degenerate boundary conditions[42]. I have thus worked upstream of the Usadel description to obtain boundary conditions valid in the case of materials with a weak spin-polarization[43]. For instance, in the limit of a weakly transparent junction between two materials L and R with a weak spin-polarization, the boundary conditions write, at side R of the junction,

$$\frac{A}{\rho_R}\check{G}_R(\vec{r})\overrightarrow{\nabla}_{\vec{r}}\check{G}_R(\vec{r}) = g_T[\check{G}_R, \check{G}_L] + g_{MR}[\check{G}_R, \{\hat{\sigma}_Z, \check{G}_L\}] - ig_\phi[\hat{\sigma}_Z, \check{G}_L] \tag{3.2}$$

with ρ_R the resistivity of material R, A the junction area, and $\hat{\sigma}_Z$ the Pauli spin operator along the magnetization direction of the junction. Above, g_T is the conductance of the junction. The conductance-like parameters g_{MR} and g_ϕ characterize the spin-polarization of tunneling amplitudes and the SDIPS (see section 2.2.2) associated to the potential barrier between the L and R materials (assuming that this barrier has a width which is much smaller than ξ_L and ξ_R). More precisely, if one writes

$$t_{n,\sigma} = \sqrt{T_n(1+\sigma P_n)}e^{i\varphi_{n,\sigma}} \tag{3.3}$$

the transmission amplitude of the barrier between L and R for the transverse propagation channel n and spin σ, one has

$$g_T = 2\sum_n T_n \tag{3.4}$$

$$g_{MR} = \sum_n T_n P_n \tag{3.5}$$

and

$$g_\phi = -2\sum_n T_n(\varphi_{n,\uparrow} - \varphi_{n,\downarrow}) \tag{3.6}$$

Note that there is a striking similarity between Eqs.(2.2) and (3.6). In fact, the g_ϕ term can induce an effective Zeeman field in a nearby normal metal[31] or superconducting layer[33, 34]. This effect is a generalization of the effect discussed in section 2.2.2 for

a single channel nanoconductor. The above work brought an important microscopic justification to the numerous references which had formerly postulated such boundary conditions[31, 32, 33, 34, 35, 36, 37, 38, 38, 40]. Very recently, I have collaborated to the generalization of these boundary conditions to the case or arbitrary spin polarizations, together with M. Eschrig at the Royal Holloway of the University of London[44]. The spin-dependent boundary conditions for the Usadel equations are now a widely used tool.

3.3 Triplet superconducting correlations in a normal metal

Triplet superconducting correlations with spin 0 have been clearly observed since about 15 years[18, 45]. However, the observation of triplet correlations with spin 1 is more recent and indirect, through the measurement of Josephson supercurrents for instance[46, 47, 48, 49]. In the work presented in this section, I have proposed a new geometry which would enable one to study more directly triplet correlations with spin one[51]. This consists in using a normal metal wire contacted to a superconductor and a ferromagnetic insulators with non-colinear magnetic domains (see Figure 3.1a). The superconductor tends to induce singlet superconducting correlations in the nanowire while the two magnetic domains of the ferromagnetic insulators provoke effective Zeeman fields in the normal metal. The resulting spin-precession effect converts the singlet superconducting correlations into triplet correlations. These effects can be described by using the spin-dependent boundary conditions discussed in the previous section[43]. Superconducting correlations between opposite spins and equal spins concentrate at different energies in the electronic spectrum of the normal metal wire (see Figure 3.1b). More precisely, triplet with spin one correlations focus at zero energies whereas singlet and triplet with spin zero correlations appear at finite energies corresponding to $\pm E_s^{eff}$, with E_s^{eff} the amplitude of the effective Zeeman field induced inside the nanowire by the ferromagnetic insulator. Therefore, the two types of correlations can be discriminated by performing a tunnel measurement of the density of states in the nanowire, with tunnel contacts or a STM. Note that in the experiments performed so far, the triplet correlations are induced inside a ferromagnet, whose internal exchange field is too strong to allow for the simultaneous observation of the low energy and finite energy DOS peaks. Indeed, one has E_s^{eff} much larger than the gap of the superconductor, so that the high energy peaks are not observable. The simultaneous observation of the two features would be very useful to discriminate zero energy peaks due to spurious

effects from zero energy peaks caused by genuine triplet with spin one correlations. Furthermore, the measurement of the density of states would enable a much deeper test of the understanding of superconducting correlations than the Josephson current which is an energy-integrated quantity.

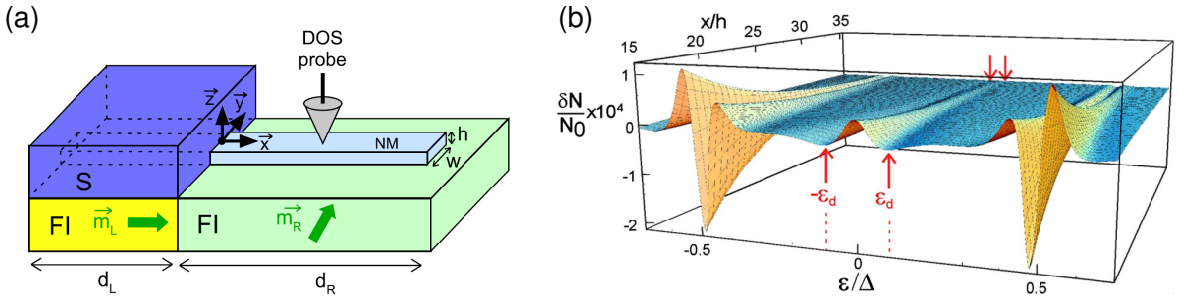

Fig. 3.1: (a) Normal metal wire (NM) contacted to two magnetic domains in a ferromagnetic insulator (FI) and to a superconductor (S). The magnetizations $\vec{m}_{L(R)}$ in the two magnetic domains are represented as green arrows. This geometry is compatible with spatially resolved DOS measurements, using a STM or several distributed tunnel contacts. (b) Difference δN between the DOS in the wire, and its normal state value N_0, versus the energy ε and the position x along the nanowire. The energy is reduced by the value Δ of the superconducting gap of S.

4. GATE CONTROLLED NANOSPINTRONICS

4.1 Introduction

The control of charge currents with electrostatic gates in electronic transistors has been a technological revolution. The spin transistor was proposed theoretically by Datta and Das in 1990 as a spintronics analogue of the conventional transistor, in which spin transport would be controlled with a gate voltage. One interest of this component is that it would allow for a further miniaturization of electronic devices, similarly to the miniaturization of data storage enabled by Magnetic Random Access Memories. The original proposal by Datta and Das suggested to obtain the spin transistor effect by using spin-orbit coupling in a nanowire[50]. However, as I reported in Section 2.2.2, spin-orbit coupling is not a necessary ingredient in the framework of quantum transport. Indeed, phase coherent nanoconductors with ferromagnetic contacts offer a natural coupling between the orbital phase of electrons and their spin, due to the existence of spin-dependent quantum interferences in the nanoconductors. Since the orbital phase of electrons can be controlled with local electric fields provided by the electrostatic gates of the nanoconductor, it is possible to build devices where spin transport in a nanoconductor is controlled electrically. This was shown during my post doc in Basel, using a carbon nanotube with two contacts magnetized in colinear directions. However, this represents only one possibility offered by phase-coherent nanospintronics. Since my arrival at LPA, I have collaborated with the HQC group on two transport experiments which aim at exploring other possibilities of this field[25, 22]. A further perspective is the spin/photon coupling demonstrated in Ref.[87], which will be discussed in section 5.7.

4.2 Multiterminal circuits

Spin-dependent quantum interference effects allow to build a spin transistor based on a carbon nanotube, as already discussed in section 2.2.2. Using more than two contacts could offer extra functionnalities in the context of a future nanospintronics. Hence,

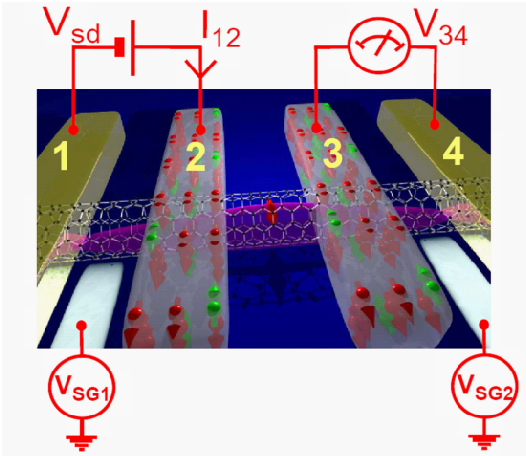

Fig. 4.1: Artist view of a non-local spin transport experiment in a carbon nanotube with two ferromagnetic contacts (2 and 3) and two normal metal contacts (1 and 4). The electric current is measured between contacts 1 and 2 and contacts 3 and 4 are left floating.

I have studied this situation theoretically, by using the Landaüer-Büttiker scattering formalism[52]. I have made predictions on several non-local measurement schemes, where an electric current is imposed between a source and a drain (1 and 2 in Fig. 4.1), and two other contacts are left floating outside the classical current trajectory (3 and 4 in Fig.4.1). I have found that, at low temperatures, the conductance between the source and drain depend on the magnetic configuration of the floating contacts. This is due to the weak number of channels in the nanoconductor and the coherent transport regime. This effect is particularly spectacular because it would not happen with multichannel diffusive conductors considered usually for non-local spin transport experiments. These predictions have been confirmed experimentally by the HQC team, using devices based on a carbon nanotube on top of which two normal metal contacts and two ferromagnetic contacts have been evaporated (thesis of Chéryl Feuillet-Palma, 2006-2010). The signals in this experiment confirm that the orbital phase and the spin of electrons can be both conserved when electrons travel in the nanotube below the metallic contacts[53].

4.3 Gate-modulated spin-precession

So far, experimental studies on spin transport in quantum dots had used only ferromagnetic contacts with colinear magnetizations. However, the non-colinear case is also very interesting because it can enable a deeper investigation of the spin dynamics in the dot. The first experimental study of a spin valve made out of a carbon nanotube and

two non-colinear ferromagnetic contacts has been realized during the thesis of Dora Crisan (2010-2013). I have participated to the theoretical interpretation of the results of this experiment. The data suggest the existence of a spin precession of electrons in the dot, due to the spin-polarized current which goes through the dot in the presence of a bias voltage. This effect is again gate-controllable[54].

5. CAVITY QED WITH HYBRID NANOCIRCUITS

5.1 Introduction

Cavity QED enables the study of the interaction between light and matter at the most elementary level, by using a two level system which interacts with a single photon trapped in a microwave cavity. This type of experiment has been realized for instance with Rydberg atoms coupled to a photonic cavity made out of high finesse superconducting mirrors[55]. Since the Rydberg atoms are naturally weakly coupled to external decoherence sources, it has been possible to realize different types of quantum manipulation of the atom/photon system. More recently, it was possible to transfer this type of experiments to superconducting chips[56]. In this case, the atoms are replaced by superconducting quantum bits and the photonic cavities are microwave cavities which can be realized for instance by using a piece of superconducting coplanar waveguide interrupted by two capacitances. One interest of this Circuit QED is that the properties of the superconducting quantum bit are not set by nature like those of an atom, but they can be chosen with the quantum bit design and accurately tuned with magnetic fluxes or gate voltages.

Since my arrival at LPA, I have made several theory proposals in order to push further Circuit QED, by replacing the superconducting quantum bits by other types of hybrid nanocircuits based on quantum dots, for instance. This possibility, called "Mesoscopic QED", was already envisioned in 2004, in a pioneering theory paper by L. Childress et al.[57]. The nanocircuits can be made out of different types of nanoconductors such as carbon nanotubes, semiconducting nanowires, or nanostructures in two-dimensional electron gases, contacted to different types of metallic reservoirs such as normal metals, superconductors, or ferromagnets. The cavity photons thus interact with systems which are much more complex than a two level system. This gives access to situations which are new in the context of Cavity QED. This also offers the possibility to study electronic transport in nanocircuits and more generally condensed matter problems under a new perspective. Indeed, the dc current which flows through a nanocircuit and the microwave response of the cavity give access to different infor-

mation. In practice, it is possible to measure simultaneously these two quantities. I have collaborated to the first experiment of this kind, realized by the HQC team with a quantum dot delimited by two normal metal contacts[58]. This work has paved the way

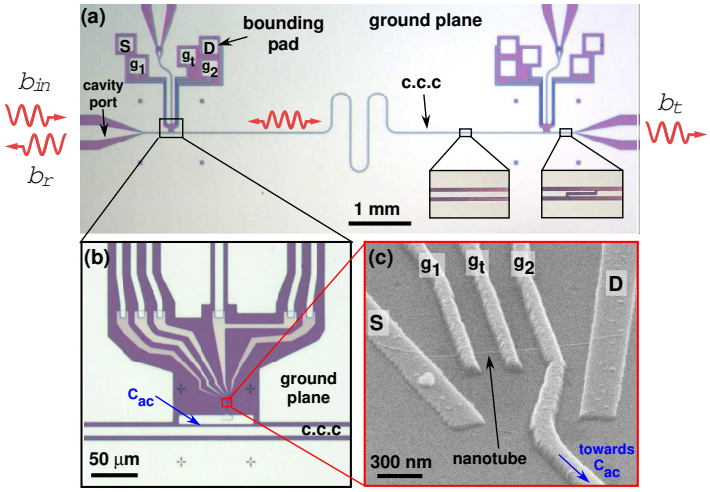

Fig. 5.1: Example of hybrid circuit QED device (a) Optical micrograph of a coplanar waveguide microwave resonator. The left inset shows a zoom on the coplanar waveguide, which is a central conductor surrounded by two ground planes. The right inset shows one of the capacitances which interrupts the waveguide to form a microwave cavity. The microwave incident, transmitted and reflected amplitudes b_i, b_t and b_r are imposed/monitored in the cavity ports which correspond to the pieces of waveguide on the other side of these capacitances. The squares are bonding pads which are isolated from the cavity ground plane and carry DC voltage or current (b) In this particular sample, an extra superconducting pad was placed next to the resonator line, providing a large coupling capacitance C_{ac} between the cavity central conductor (c.c.c.) and one of the sample gates (c) Scanning electron micrograph of the nanocircuit coupled to the cavity, here a single wall carbon nanotube (SWNT) connected to source and drains (S and D) reservoirs as well as three top gates g_1, g_2 and g_T.

to a vast class of experiments which combine microwave cavities and hybrid nanocircuits. Note that other types of experiments study quantum dots coupled to optical cavities[59, 60]. I will not consider this possibility here because in these experiments, the quantum dots are isolated and thus do not form an electronic circuit.

5.2 Physical implementation of the nanocircuit-photon coupling

The combination of hybrid nanocircuits with coplanar microwave cavities pushes further the on-chip design initially introduced in the context of Circuit QED experiments to control and readout the state of a superconducting quantum bit[56]. Many

different types of nanoconductors have already been embedded in coplanar cavities, such as lateral quantum dots defined on GaAs/AlGaAs heterostructures[61, 62] or Si/SiGe heterostructures[63, 64], quasi-one dimensional conductors such as carbon nanotubes[58, 65], InAs nanowires[66, 67, 68], or InSb nanowires[69], but also graphene quantum dots[70] and atomic contacts[71]. Different types of metallic contacts can be used, such as normal metals, superconductors [72] and ferromagnets with collinear[73] or non-collinear magnetizations[54, 74]. Therefore, a large variety of geometries and situations can be studied. Figure 5.1 shows an example of Mesoscopic QED sample. There, the hybrid nanocircuit is a double quantum dot fabricated out of a carbon nanotube on top of which source (S), drain (D), and top gates (g_1, g_2 and g_T) have been evaporated (Fig.5.1c). The double dot is coupled capacitively to the cavity central conductor (c.c.c.), through the capacity C_{ac}, near a cavity electric field antinode (Fig.5.1b). The cavity central conductor is interrupted by on-chip capacitances such as the one visible in the right inset of Fig.5.1a. Openings are fabricated across the cavity ground plane to allow for an electric connection of the source, drain and gate electrodes of the double dot at bonding pads visible as squares in Fig.5.1a.

5.3 Theoretical description of the nanocircuit-photon coupling

5.3.1 Comparison between the different types of cavity QED experiments

The description of the electron/photon coupling requires to take into account various specificities of nanocircuits[75]. First, since these nanocircuits are much bigger than an atom, one has to take into account that there exists strong spatial variations of the cavity electric field on the scale of the nanocircuit. These field variations can be increased on purpose, for instance by coupling only one dot in a double quantum dot to the cavity central resonator, through a capacitive connection (see Fig.5.2c for instance). Another source of field variations is field screening inside the metallic reservoirs of the nanocircuit. These field inhomogeneities are reminiscent from those which occur in a superconducting quantum bit. Second, one has to take into account the existence of discrete orbital states, which exist in a confined portion of nanoconductor such as a quantum dot. This individual orbital degree of freedom is reminiscent from the orbital degree of freedom in an atom. It has no equivalent in superconducting quantum bits where only macroscopic collective variables such as the total charge of a superconducting island are relevant, due to the rigidity of the superconducting phase.

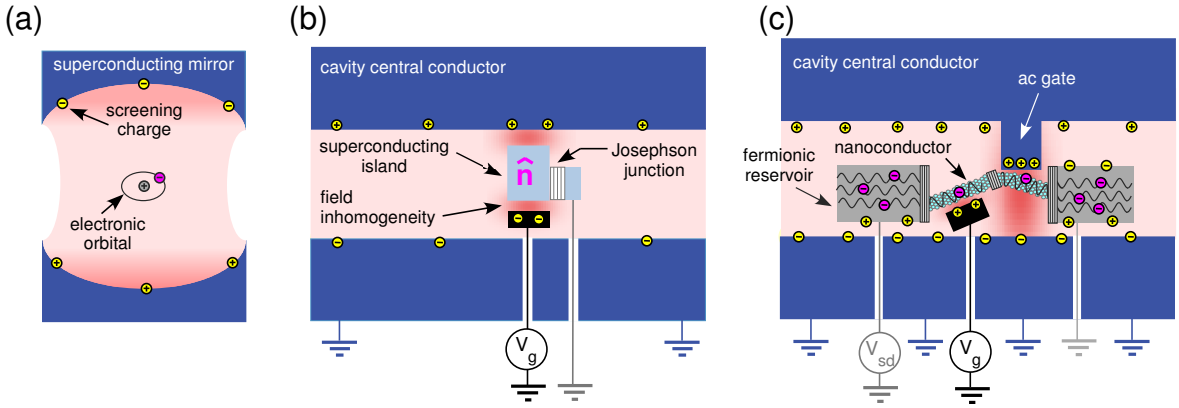

Fig. 5.2: Schematic representation of the different types of cavity QED experiments (a) Cavity QED experiment with an atom (b) Circuit QED experiment with a charge superconducting quantum bit (c) Mesoscopic QED experiment with a hybrid nanocircuit. Cavity conductors are represented in blue and dc electrostatic gates in black. The photonic field is presented in pink, with inhomogeneities in dark pink. Electronic charges occupying orbitals of the flying atom in panel a, or tunneling between quasi-localized orbitals of the nanocircuit in panels c, are represented in fuchsia. Plasmonic screening charges on the metallic elements are represented in yellow.

Finally, one has to take into account collective plasmonic modes which exist in the metallic reservoirs. These modes are only implicitly taken into account in the usual description of superconducting Circuit QED, through current conservation. In the case of nanocircuits, this task is a priori not trivial since fermionic reservoirs host simultaneously plasmonic modes *and* individual fermionic quasiparticle modes which cause quantum transport effects in the nanocircuit. These quasiparticle modes are coupled to the localized discrete electronic orbitals inside the nanoconductors through tunnel junctions.

5.3.2 Minimal coupling Hamiltonian

In order to take into account both quasiparticle tunneling and plasmonic screening in a minimal way, one can assume that the plasmonic screening charges in fermionic reservoirs have a frequency which is much higher than all the other relevant frequencies in the device. In this case, they simply renormalize the cavity field and carry displacement currents enslaved to tunneling events. This is why, in Ref.[75], performed in collaboration with T. Kontos and B. Douçot, we have not described explicitly plasmons. Instead, we have taken into account their effect through effective boundary conditions which modify the spatial profile of the photonic field and the Coulomb interactions in the

nanocircuit. We refer the interested readers to Ref.[75] for the detailed quantization procedure of the system electromagnetic field. We obtain

$$\hat{H}_{tot} = \hat{H}_0 + \omega_0 \hat{a}^\dagger \hat{a} \tag{5.1}$$

with

$$\hat{H}_0 = \int d^3r \hat{\psi}^\dagger(r) h_\rho(\vec{r}) \hat{\psi}(\vec{r}) + \hat{H}_{Coul} \tag{5.2}$$

$$+ \int d^3r \left(\Delta(\vec{r}) e^{2\Phi(\vec{r},\hat{a},\hat{a}^\dagger)} \hat{\psi}^\dagger_\uparrow(\vec{r}) \hat{\psi}^\dagger_\downarrow(\vec{r}) + H.c. \right) \tag{5.3}$$

and

$$h_\rho(\vec{r}) = \frac{1}{2m} \left(-i\hbar \overrightarrow{\nabla}_{\vec{r}} + e \overrightarrow{\hat{A}}(\vec{r}) \right)^2 - eV(\overrightarrow{r}) \ , \tag{5.4}$$

Above, one has $\hat{\psi}^\dagger(\vec{r}) = (\hat{\psi}^\dagger_\uparrow(\vec{r}), \hat{\psi}^\dagger_\downarrow(\vec{r}))$, with $\hat{\psi}^\dagger_\sigma(\vec{r})$ the field operator associated to the creation of electronic quasiparticles with spin σ in the nanocircuit. The term $\widetilde{h}_\rho(\vec{r})$ is the single particle Hamiltonian which includes the light-matter interaction through the photonic vector potential term

$$\overrightarrow{\hat{A}}(\vec{r}) = \vec{\mathcal{A}}(\vec{r}) i(\hat{a} - \hat{a}^\dagger) \ , \tag{5.5}$$

The potential $V(\overrightarrow{r})$ takes into account the confinement of conduction electrons in the nanocircuit, i.e. the effect of the materials crystalline background, treated in the mean field approach, and the capacitor fields due to the dc electrostatic gates. The term in $\Delta(\vec{r})$ of Eq.(5.2) is a pairing term which describes superconducting correlations in the nanocircuit. This term must include a phase factor $\Phi(\vec{r}, \hat{a}, \hat{a}^\dagger)$ which depends on the photonic creation and annihilation operators $\hat{a}^\dagger$ and $\hat{a}$, in order to ensure the gauge invariance of the Hamiltonian.

5.3.3 Photonic pseudo-potential picture

Different types of light-matter interactions appear in Hamiltonian (5.1). Indeed, Eq.(5.4) contains a linear term in $\overrightarrow{\nabla}_{\vec{r}}.\overrightarrow{\hat{A}}(\vec{r})$ and a non linear term in $\hat{A}^2$. It also contains the exponential of the phase factor $\Phi(\vec{r}, \hat{a}, \hat{a}^\dagger)$ which is non-linear. The effect of the non-linear terms is not negligible, in principle (see Appendix B of Ref.[75] for details). Therefore, in this section, we introduce a unitary transformation of the Hamiltonian $\hat{H}_{tot}$ which greatly simplifies the form of the light-matter interaction. Note that analogous transformations have been used in atomic Cavity QED for cavity fields with a limited spatial variation, such as the Power–Zienau–Woolley transformation[76]. However, these transformations are not directly applicable in our case since strong spatial variations of the photonic fields can occur due to local ac gates and screening effects.

For simplicity, we consider nanocircuits with standard dimensions and without loops, so that one can disregard magnetic effects induced by the photons. This means that one can use $\vec{\nabla}_{\vec{r}} \wedge \overrightarrow{A} \simeq 0$ on the scale of the whole nanocircuit. This assumption is valid for all the Mesoscopic QED devices studied experimentally so far, except Ref.[71]. This case will be discussed elsewhere. When $\vec{\nabla}_{\vec{r}} \wedge \overrightarrow{A} \simeq 0$, it is possible to define a photonic pseudo potential $V_{\perp}(\overrightarrow{r})$ such that

$$\vec{\nabla}_{\vec{r}}.V_{\perp}(\overrightarrow{r}) \simeq \omega_0 \vec{\mathcal{A}}(\vec{r}) \tag{5.6}$$

and

$$\hat{\Phi}(\vec{r}) = e(\hat{a} - \hat{a}^{\dagger})V_{\perp}(\overrightarrow{r})/\omega_0 \tag{5.7}$$

Then, one can apply to Hamiltonian (5.1) the unitary transformation $\tilde{H}_{tot} = \mathcal{U}^{\dagger}\hat{H}_{tot}\mathcal{U}$ with

$$\mathcal{U} = \exp\left(\frac{e(\hat{a} - \hat{a}^{\dagger})}{\omega_0}\hat{\mathcal{V}}\right) \tag{5.8}$$

and

$$\hat{\mathcal{V}} = -e\int d^3r V_{\perp}(\overrightarrow{r})\hat{\psi}^{\dagger}(\vec{r})\hat{\psi}(\vec{r}) \tag{5.9}$$

This leads to [75]

$$\tilde{H}_{tot} = H_0' + \hat{\mathcal{V}}(\hat{a} + \hat{a}^{\dagger}) + \omega_0\hat{a}^{\dagger}\hat{a} \tag{5.10}$$

with

$$\begin{aligned} H_0' = &\int d^3r\hat{\psi}^{\dagger}(r)h_{\rho}'(\vec{r})\hat{\psi}(\vec{r}) + \hat{H}_{Coul} \\ &+ (\hat{\mathcal{V}}^2/\omega_0) + \int d^3r\left(\Delta(\vec{r})\hat{\psi}_{\uparrow}^{\dagger}(\vec{r})\hat{\psi}_{\downarrow}^{\dagger}(\vec{r}) + H.c.\right) \end{aligned} \tag{5.11}$$

$$h_{\rho}'(\vec{r}) = -\frac{\hbar^2}{2m}\Delta_{\vec{r}} - eV(\overrightarrow{r}) \ , \tag{5.12}$$

and

$$\hat{\mathcal{V}} = -e\int d^3r V_{\perp}(\overrightarrow{r})\hat{\psi}^{\dagger}(\vec{r})\hat{\psi}(\vec{r}) \tag{5.13}$$

This above description which is particularly simple since it only involves only a linear coupling between the individual electronic states in the nanocircuit and a scalar photonic potential $V_{\perp}(\overrightarrow{r})$. Interestingly, the above Hamiltonian bridges between Cavity QED and Circuit QED. Indeed, the usual dipolar electric approximation of Cavity QED corresponds to a photonic potential which evolves linearly in space i.e. $V_{\perp}(\overrightarrow{r}) = \overrightarrow{\hat{E}}_0.\overrightarrow{r}$, whereas Circuit QED corresponds to a constant photonic potential inside each node of the circuit model.

5.4 Anderson-like Hamiltonian for Mesoscopic QED

Since tunneling physics is at the heart of quantum transport, it is useful to reexpress Hamiltonian (5.10) to describe tunneling explicitly. For this purpose, one needs to decompose the field operator $\hat{\psi}^\dagger(\vec{r})$ associated to quasiparticles modes of the black circuit on the ensemble of the creation operators $\hat{c}_n^\dagger$ for electrons in an orbital n with energy ε_n of a given circuit element (reservoir, dot,...). At lowest order in tunneling, one can use $\hat{\psi}^\dagger(\vec{r}) = \varphi_n^* \hat{c}_n^\dagger$[77]. Then, Hamiltonian (5.10) directly gives

$$\hat{H}_{tot} = \hat{H}_0 + \hat{h}_{int}(\hat{a} + \hat{a}^\dagger) + \omega_0 \hat{a}^\dagger \hat{a} \tag{5.14}$$

with

$$\hat{H}_0 = \sum_n \varepsilon_n \hat{c}_n^\dagger \hat{c}_n + \sum_{n \neq n'} (t_{n,n'} \hat{c}_{n'}^\dagger \hat{c}_n + H.c.) \tag{5.15}$$

$$\hat{h}_{int} = \sum_n g_n \hat{c}_n^\dagger \hat{c}_n + \sum_{n,n'} (\gamma_{n,n'} \hat{c}_{n'}^\dagger \hat{c}_n + H.c.) \ . \tag{5.16}$$

$$g_n = -e \int dr^3 \left|\varphi_n(\vec{r})\right|^2 V_\perp(\vec{r}) \ . \tag{5.17}$$

and

$$\gamma_{n',n} = -e \int dr^3 \varphi_n^*(\vec{r}) \varphi_{n'}(\vec{r}) V_\perp(\vec{r}) \tag{5.18}$$

Above, $\hat{H}_0$ is the Anderson-like Hamiltonian of the nanocircuit, with $t_{n,n'}$ the tunnel coupling between orbitals n and n', which is finite only if n and n' correspond to two orbitals in two different circuit elements coupled through a tunnel junction. The term $\hat{h}_{int}(\hat{a} + \hat{a}^\dagger)$ describes the nanocircuit-photon interaction. Cavity photons can have two different effects. First, they can shift the energy of orbital n due to the term in g_n. In this report, I will mainly discuss the effects of the g_n elements which are expected to be dominant in most mesoscopic QED devices and have been sufficient to interpret experiments, so far. However, in principle, cavity photons can also induce direct transition terms between two different orbitals of the nanocircuit, due to the term in $\gamma_{n',n}$. Nevertheless, from Eq.(5.18), the terms $\gamma_{n',n}$ are expected to be weak because $\varphi_n(\vec{r})$ and $\varphi_{n'}(\vec{r})$ have a small matrix element in general. I will discuss a situation where the $\gamma_{n',n}$ term becomes relevant in section 5.9.

5.5 Theoretical description of the cavity signals in the semiclassical linear limit

The cavity signals can be expressed in a simple way in the semiclassical limit where the number of photons in the cavity is sufficiently large (> 10) to disregard quantum

fluctuations of the cavity field. To describe most experiments performed so far, one can furthermore describe the nanocircuit/photon coupling with a linear response approach, which requires that this photon number is also not too large (typically, $n < 500$). Following the discussion in section 5.4, one can finally assume that the light-matter interaction is well approximated by

$$\hat{h}_{int} = \sum_n g_n \hat{c}_n^\dagger \hat{c}_n \tag{5.19}$$

The cavity microwave response is measured by using input and output ports which correspond to the pieces of waveguide connected capacitively to the cavity, on both sides of the cavity central conductor (see Fig.5.1a). In the semiclassical limit, the incident, transmitted and reflected photon fluxes in these ports can be characterized by complex amplitudes b_{in}, b_t and b_r. We assume that the cavity is excited through the left port in Fig.5.1, which will be considered as the input port. The transmission b_t/b_{in} of the cavity can be obtained experimentally by measuring the microwave amplitude b_t going out through the output port, which can be the right port in Fig.5.1. With the above assumptions, the cavity microwave transmission can be expressed as[72]

$$\frac{b_t}{b_{in}} = \frac{2\sqrt{\Lambda_L \Lambda_R}}{\omega_{RF} - \omega_0 + i\Lambda_0 - \Xi(\omega_{RF})} \tag{5.20}$$

Above, $\Lambda_{L(R)}$ corresponds to the contribution of the left(right) port to the cavity linewidth Λ_0, which implies $\Lambda_L + \Lambda_R \leq \Lambda_0$. The global charge susceptibility $\Xi(\omega_{RF})$ of the nanocircuit is defined as

$$\Xi(\omega_{RF}) = \sum_{n,n'} g_n g_{n'} \chi_{n,n'}(\omega_{RF}) \tag{5.21}$$

with

$$\chi_{n,n'}(t-t') = -i\theta(t-t') \left\langle [\hat{c}_n^\dagger(t)\hat{c}_n(t), \hat{c}_{n'}^\dagger(t')\hat{c}_{n'}(t')] \right\rangle_{\hat{h}_{int}=0} \tag{5.22}$$

Above, $\langle\rangle_{\hat{h}_{int}=0}$ denotes the statistical averaging with $g_n = 0$ for any n.

In practice, the experimental signals which are directly measured are the phase shift $\Delta\varphi$ and amplitude shift ΔA of the transmission b_t/b_{in}, caused by the presence of the nanoconductor. One can write

$$\frac{b_t}{b_{in}} = (A_0 + \Delta A) e^{i(\varphi_0 + \Delta\varphi)} \tag{5.23}$$

However, it is often convenient to discuss the cavity frequency shift $\Delta\omega_0$ (dispersive signal) and cavity linewidth shift Λ_0 (dissipation signal) caused by the presence of the nanocircuit. From Eq.(5.23), in the limit $\omega_{RF} = \omega_0$ and $|\Delta\omega_0|, |\Delta\Lambda_0| \ll |\omega_0|, |\Lambda_0|$

which is often used experimentally, the signals ΔA and $\Delta\varphi$ are directly related to the cavity parameters' shifts, i.e.

$$\Delta\varphi = \frac{\Delta\omega_0}{\Lambda_0} = \mathrm{Re}[\Xi(\omega_0)]\frac{1}{\Lambda_0} \tag{5.24}$$

and

$$\Delta A = -\frac{\Delta\Lambda_0 A_0}{\Lambda_0} = -\,\mathrm{Im}[\Xi(\omega_0)]\frac{A_0}{\Lambda_0} \tag{5.25}$$

so that $\Delta\varphi$ and ΔA correspond to the dispersive and dissipative parts of the cavity response $\Delta\omega_0$ and $\Delta\Lambda_0$, respectively. Beyond this limit, the experimental data can be modeled by combining Eqs.(5.20) and (5.23).

Depending on the regime of parameters fulfilled by the nanocircuit, and in particular the order of magnitude of the tunnel rates between the dots and reservoirs, different calculation techniques can be used to calculate $\Xi(\omega_0)$. I will discuss several possibilities in the next sections. In this report, I will only consider cases where the summation on indices n and n' in Eq.(5.21) can be restricted to internal sites of the nanoconductor. This requires that the coupling between the cavity and the nanoconductor sites is much larger than the coupling between the cavity and the reservoirs. This is not a priori obvious since the nanoconductor is much smaller than the reservoirs and thus tends to have a smaller capacitance towards the cavity resonator. However, this feature can be compensated by using for instance ac top gates which reinforce the coupling between the nanoconductor and the cavity. A careful work has been done in the HQC group to reach this situation[74, 72, 78]. In this limit, $\Xi(\omega_0)$ corresponds to the charge susceptibility of the nanoconductor at frequency ω_0. In the opposite limit, it has been observed experimentally that the cavity signals essentially show replicas of the conductance signal[58].

5.6 Double quantum dot with normal metal reservoirs

The case of a double quantum dot embedded in a microwave cavity has received most experimental attention so far (see for instance Refs.[61, 79, 66, 81, 82, 62]). I will note L and R the two dots in a double dot. The intrinsic level separation Δ_o (see Eq.2.3) between the orbitals of one dot is usually very large in comparison with the cavity frequency. Therefore, it is sufficient to consider a single orbital with energy $\varepsilon_{L(R)}$ in dot $L(R)$. These two orbitals are coupled with a hopping constant t through a tunnel barrier (see Fig.5.3b). It is possible to tune the gate voltages V_g^L and V_g^R of the two dots such that there is a single electron in the double dot due to Coulomb blockade.

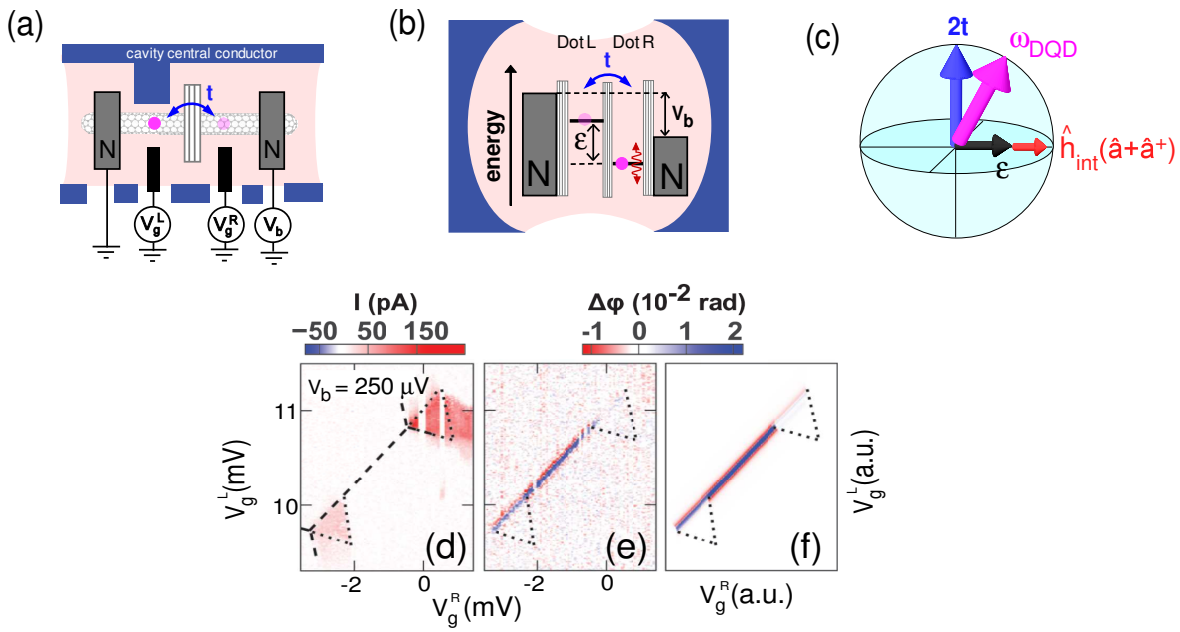

Fig. 5.3: (a) Schematic representation of a double dot made in a carbon nanotube, and delimited by two normal metal contacts and a central barrier with a hoping constant t. The energy of the dot orbitals can be tuned with the gate voltages $V_g^{L(R)}$ and the right reservoir is biased with a voltage V_b . The cavity conductors are represented in blue (b) Energy diagram of the double dot. The energy detuning between the left and right dot orbitals is ε. The microwave cavity is represented schematically by mirrors in blue (c) Effective bloch sphere representing the internal state of the double dot. The unperturbed dot Hamiltonian $\hat{H}_0$ corresponds to the magenta field with modulus ω_{DQD}, which is the sum of the blue and black fields which represent 2t and ε respectively. The coupling to the cavity is represented by the red field (d) dc current through a carbon-nanotube double quantum dot versus the gate voltages V_g^L and V_g^R for a finite bias voltage $V_b = 250\mu V$. (e) Corresponding cavity signal $\Delta\varphi$ (f) Theoretical predictions for $\Delta\varphi$, obtained with Eq.(5.31) and a master equation calculation of n_+ and n_- at zeroth order in g_t.

In the absence of magnetic field or ferromagnetic materials, the spin degree of freedom can be disregarded to describe this situation since the two spin species play the same role and are not present simultaneously in the double dot. Therefore, the only internal degree of freedom relevant to describe the internal dynamics of the double dot in this limit is the left/right charge degree of freedom. In this framework, the double dot Hamiltonian writes

$$\hat{H}_0 = \frac{\varepsilon}{2}(\hat{c}_L^\dagger \hat{c}_L - \hat{c}_R^\dagger \hat{c}_R) + t\hat{c}_L^\dagger \hat{c}_R + t^* \hat{c}_R^\dagger \hat{c}_L + \hat{H}_{Coul} \tag{5.26}$$

where $\hat{H}_{Coul}$ forbids the double occupation of the double dot, $\hat{c}_{L(R)}^\dagger$ is the creation operator for an electron in dot $L(R)$ and $\varepsilon = \varepsilon_R - \varepsilon_L$ the dot orbital detuning. Using the basis of bonding and antibonding states of the double dot, one gets

$$\hat{H}_0 \simeq \frac{\omega_{DQD}}{2}(\hat{c}_-^\dagger \hat{c}_- - \hat{c}_+^\dagger \hat{c}_+) + \hat{H}_{Coul} \tag{5.27}$$

with $\omega_{DQD} = \sqrt{\varepsilon^2 + 4t^2}$ the double dot transition frequency. Above, we have used the creation operators

$$\hat{c}_+^\dagger = \cos[\theta/2]\hat{c}_L^\dagger + \sin[\theta/2]\hat{c}_R^\dagger \tag{5.28}$$

and

$$\hat{c}_-^\dagger = -\sin[\theta/2]\hat{c}_L^\dagger + \cos[\theta/2]\hat{c}_R^\dagger \tag{5.29}$$

for bonding and antibonding states, and the parameter $\theta = \arctan[2t/\varepsilon]$. In practice, each dot is also contacted to a normal metal reservoir, which enables one to control and measure the double dot charge (see Fig.5.3a). The orbital detuning ε can be controlled with V_g^L and V_g^R. In most experiments performed so far, the samples have been designed with asymmetric couplings $g_R \neq g_L$ of the two dots to the cavity, in order to modulate the parameter ε with the cavity electric field. This is obtained by connecting only one of the dots to the cavity central resonator with an ac gate. This gives a light-matter coupling term

$$\hat{h}_{int} = g_L \hat{c}_L^\dagger \hat{c}_L + g_R \hat{c}_R^\dagger \hat{c}_R \tag{5.30}$$

In this case, using a master equation approach, valid for tunnel rates $\Gamma_{L(R)}$ to the left and right reservoirs much smaller than the temperature $k_b T$, one finds

$$\Xi(\omega_{RF}) = \frac{g_t^2(n_- - n_+)}{\omega_{RF} - \omega_{DQD} + i\Gamma_2^*} \tag{5.31}$$

with

$$g_t = \frac{g_R - g_L}{2} \frac{2t}{\sqrt{4t^2 + \varepsilon^2}} \tag{5.32}$$

Above, Γ_2^* is the decoherence rate of the double dot transition and $n_{-/+}$ are the average populations of the bonding/antibonding states. Physically, the charge susceptibility of Eq.(5.31) is finite due to fact that the effective coupling g_t between the double dot and the cavity corresponds to a transverse coupling. This means that, in the Bloch sphere representation of the double dot Hamiltonian (see Fig.5.3c), the coupling term (5.30) corresponds to a field (in red) which has a component perpendicular to the double dot unperturbed field with modulus ω_{DQD} (in magenta). Therefore, the double dot and cavity can exchange photons, which leads to Eq.(5.31).

Equation (5.31) corresponds to a well known result of cavity and circuit QED in the dispersive regime $\omega_{RF} - \omega_{DQD} \gg \Gamma_2^*$ where Γ_2^* can be disregarded (see for instance Refs.[56, 80]). In this limit, depending on whether the nanocircuit is in the state $+$ or $-$, the cavity shows a frequency pull $\Delta\omega_0 = \pm g_t^2/(\omega_{RF} - \omega_{DQD})$. If g_t is strong enough, this can be used to read out the state of the double dot in a nondestructive way. Indeed, for $\omega_{RF} - \omega_{DQD} \gg \Gamma_2^*$, the susceptibility $\chi(\omega_{RF})$ accounts for second order processes which do not change the state of the nanocircuit. This method is widely used to read out the state of superconducting quantum bits[56].

In standard circuit QED experiments, no dc current transport occurs. In our case, from Eq.(5.31), current transport in the double dot can modify the cavity signals by modifying the populations n_- and n_+ of the bonding and antibonding states. More precisely, the microwave cavity can be used to have a direct access to the population imbalance $n_- - n_+$ caused by dc transport. Importantly, the dc current through the double dot and the cavity signals are qualitatively different, since the current I though the double dot is a more complex combination of n_-, n_+ and the double dot parameters. Figure 5.3d and 5.3e presents experimental results obtained with a carbon nanotube double quantum dot with a finite Coulomb interaction [87]. The transport configuration can be tuned electrically through the double dot gate voltages V_g^L and V_g^R and source-drain bias voltage V_b. As observed usually, the current I through the double dot is finite inside some triangles in the $V_g^L - V_g^R$ plane where the bonding or antibonding states are located inside the transport window opened by the source-drain voltage V_b (Fig.5.3d). Strikingly, the cavity signal $\Delta\varphi$ looks very different. It is maximum along the line $\varepsilon = 0$ where $\omega_{DQD} - \omega_0$ is minimum (Figs.5.3e), and it takes a different value along the transport triangles, because the populations of n_- and n_+ are modified by transport. As shown in Fig.5.3f, we could reproduce this behavior by using Eq.(5.31), with n_- and n_+ calculated with a master equation approach at lowest order in the light

matter coupling ($g_t = 0$) (see details in Ref.[87]). With this approach, we evaluate $g_t(\varepsilon = 0)/2\pi = (g_L - g_R)/2\pi = 3.3$ MHz and $\Gamma_2^*/2\pi = 345$ MHz at $\varepsilon = 0$, which has to be compared with $\Lambda_0 = 0.96$ MHz (see below).

Note that in the above experiment, one has $\Lambda_0 < g_t < \Gamma_2^*$. It is necessary to reach the strong coupling regime $g_t > \Gamma_2^*, \Lambda_0$ in order to perform an efficient coupling and readout of the double dot charge state with the techniques of Circuit QED. This regime has been reached very recently in the HQC group with my collaboration[84], as well as in Princeton and Zurich [64, 85], in double dots based on a carbon nanotube, a Si/SiGe heterostructure and a GaAs/AlGaAs heterostructure, respectively. Two different recipes can be used to obtain the strong coupling regime: one can either increase g_t [85] or decrease Γ_2^* [64, 84]. However, I will not discuss these experiments in details here. In the next sections, I will rather show that other degrees of freedom than the L/R charge degree of freedom of a double quantum dot can also give interesting results in the context of Mesoscopic QED.

5.7 Coherent coupling between a single spin and cavity photons

The use of electronic spins confined in nanoconductors is a priori very appealing in the context of quantum information, because spins are less sensitive to decoherence effects than charge degrees of freedom. However, this goes together with a huge technical challenge because the natural magnetic coupling between spins and photons is extremely weak (a few 10Hz). In order to solve this problem, I have developed theoretically, together with T. Kontos, a new type of spin quantum bit based on a double quantum dot with two ferromagnetic contacts magnetized in non-colinear directions[86] (see Fig.5.4a). A similar device had been formerly considered theoretically in the context of the study of spin-dependent transport[91]. Here, we consider the limit of vanishing tunnel rates so that each ferromagnetic contact essentially produces in the nearby quantum dot an effective Zeeman field similar to the one of Eq.(2.2). Thanks to Coulomb blockade, one can tune the dc gates of the device such that the double dot contains only one electron. The occupation of the two dots by this electron depends on the value of the orbital level detuning ε between the two dots. Therefore, due to the non-colinearity of the effective Zeeman fields in the two dots, one can vary the direction of the global effective field seen by this electron by changing ε. Since ε can be modulated by the cavity electric field, a transverse spin/photon coupling is obtained. This coupling should in principle enable one to use the techniques of Circuit QED to

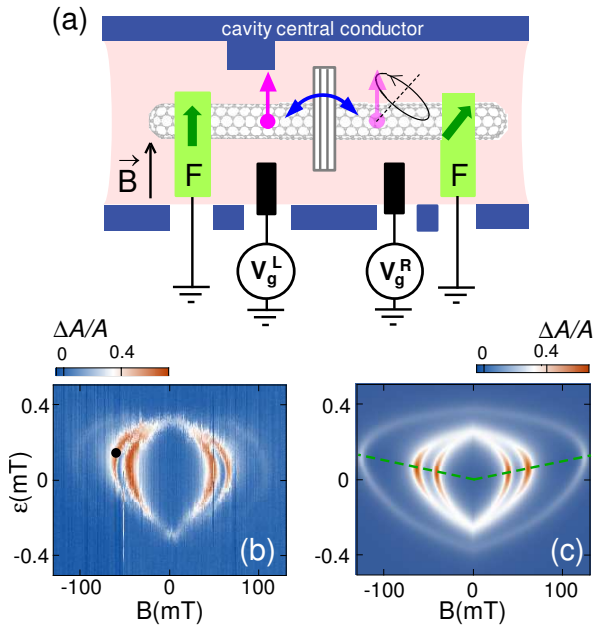

Fig. 5.4: Response of a microwave cavity coupled to a double quantum dot with non colinear ferromagnetic contacts. The double dot is represented schematically in panel (a). The cavity dissipation of panel (b) displays various resonances which dependent on the orbital detuning ε of the double dot and the applied magnetic field B. This signal is reproduced theoretically in panel (c) (see text). The green dotted line corresponds to a sweet line with respect to charge noise.

readout the state of a single spin or couple two distant spins through the exchange of virtual cavity photons[80]. Another interest of this geometry is that the spin/photon coupling can be switched off by using a large value of ε such that the electron is trapped in a single dot and does not feel anymore the non-colinearity of the contacts magnetizations. This should enable one to reduce the spin decoherence caused by the coupling to the cavity outside of the spin manipulation periods. Therefore, the setup of Fig.5.4a could also be used as a quantum memory, in principle.

The first implementation of this device has been realized during the theses of Jérémie Viennot (2010-2014), and Matthieu Dartiailh (beginning : 2013), with my support for data modelling[74]. When the microwave transmission amplitude of the cavity is measured versus ε and the external magnetic field B applied to the double dot, three resonant lines appear (see Fig.5.4b). Various features suggest that the spin degree of freedom is an important ingredient in this pattern. First, the resonances split and strongly move with the external magnetic field B, with a maximum of contrast/coherence for a finite value of B. Second, the black point of Fig.5.4b corresponds to a coupling $g_s = 1.3$ MHz and a double dot decoherence rate $\Gamma_2^*/2\pi = 2.5$ MHz. This

last number is about 200 times smaller than the charge decoherence rate determined for a similar carbon nanotube device (see section 5.6). This device is almost in the strong coupling regime.

To understand better the contribution of the spin degree of freedom in the cavity signals, one can calculated the charge susceptibility of the device with a generalization of Eq.(5.31). This gives

$$\Xi(\omega_{RF}) \simeq \sum_{ij} \frac{g_{ij}^2 (n_j - n_i)}{\omega_{RF} - \omega_{ij} + i\Gamma_{ij}} \tag{5.33}$$

Above, ω_{ij} is an internal transition frequency of the nanoconductor between states i and j, Γ_{ij} is the decoherence rate associated to this transition, and n_i is the average occupation of state i. This expression is valid for $\Gamma_{ij} \ll k_B T$ and all transitions frequencies of the device well separated. To calculate the frequencies ω_{ij} and the couplings g_{ij}, we have used a double dot Hamiltonian which takes into account the existence of the left/right and spin degree of freedoms of the double dot, but also the K/K' local orbital degree in each dot (or valley degree of freedom), which is due to the fact that electrons can rotate clockwise or anticlockwise around the carbon nanotube. The linewidth of the resonances can be modeled by taking into account the effect of charge noise which is due to charge fluctuators moving in the vicinity of the double dot, similarly to what happens for the Quantronium circuit of section 2.1. Charge noise induces fluctuations of the transitions frequencies ω_{ij} which cause a dephasing effect. Using Eq.(5.33), we have obtained Fig.5.4c, which reproduces well the behavior of Fig.5.4b. The two strongest resonances mainly correspond to spin transitions with a conserved K/K' index. These two resonances are slightly split due to a small lifting of the K/K' degeneracy. The third weaker resonance mainly corresponds to a transition where both the spin and the K/K' index are reversed. In Fig.5.4c, this transition is less visible than the two others because the K/K' degree of freedom is only weakly coupled to cavity photons. In practice, the coupling of K/K' to the cavity can be due to microscopic disorder in the carbon nanotube structure[89, 88]. This third resonance is interesting in the light of a recent theory proposal which suggests to couple the valley degree of freedom of a Si dot to a microwave cavity [90]. Remarkably, the coherence (or, visually, the contrast) of the three transitions is maximum along the green dashed line in Fig.5.4c. This is because the derivative of the transition frequencies ω_{ij} with respect to ε vanishes along this line, so that the effect of charge noise is minimal. In other terms, this line represents a sweet line for charge noise, in full analogy with the sweet spot of the Quantronium circuit of section 2.1. This behavior also occurs in the

data, which confirms that charge noise is an important source of decoherence in our device. It should be possible to increase the performances of this device by reducing the spin-charge hybridization to decrease decoherence due to charge noise. It is expected that decoherence will decrease more quickly than g_s with ε, so that the strong coupling regime is accessible with this geometry, in principle[86].

Interestingly, there exists alternative theory proposals to couple the spin degree of freedom of a quantum dot circuit to a coplanar microwave cavity. One may use spin-orbit coupling or inhomogeneous stray fields to couple a single electron spin state to cavity photons[92, 93, 94, 95, 96, 86]. Alternatively, one could use two or three electron states in a multi-quantum dot circuit with proper spin-symmetry breaking ingredients, so that the spin/photon coupling occurs without any individual spin precession effect[98, 99, 97, 100, 101, 102, 103, 104]. Note that on the experimental level, the strong spin-photon coupling has also been obtained recently in a quantum dot coupled to an optical microcavity in a semiconductor nanopillar[105]. More precisely, a single hole spin in the quantum dot is coupled to the polarization of the cavity photons. In our case, the polarization is not a relevant quantity due to the geometry of our cavities which imposes the directions of the cavity electric and magnetic fields.

5.8 Single quantum dot contacted to fermionic reservoirs

So far, I have discussed experiments, where the cavity signals are dominated by resonances between the cavity mode and internal transitions of a double dot. This effect is described by Eq. (5.33) which also holds for a superconducting qubit in a miccrowave cavity. To exploit fully the specificities of nanocircuits, it is interesting to bring dot-reservoirs tunnel transitions in resonance with the cavity. This can lead to a large variety of effects. For instance, a single quantum dot coupled to both a superconducting reservoir and a normal metal reservoir with a bias voltage can emit cavity photons. This effect is due to inelastic tunnel processes between the dot and a BCS peak in the density of states of the superconducting contact. During her thesis (2013-2016), Laure Bruhat has observed this effect[72]. Figure 5.5a shows the amplitude of the cavity microwave transmission, measured versus the source drain voltage V_b applied on the normal metal contact and the dot gate voltage V_g. The main red line corresponds to the resonance between the dot level and the Fermi level in the normal metal reservoir, as sketched in panel 1, and the paler red lines to the resonances between the dot level and the BCS peaks in the density of states of the superconducting reservoir, as

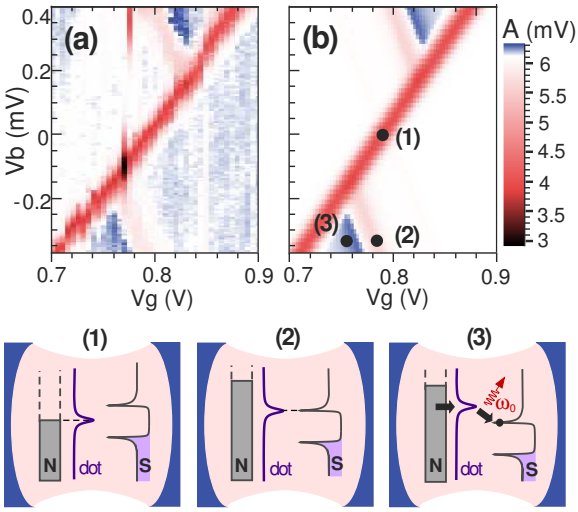

Fig. 5.5: (a) Microwave transmission amplitude measured for a cavity coupled to a superconductor/quantum dot/normal metal bijonction. The white shade corresponds to the reference amplitude $A_0 = 6.1$ mV and the blue and red shades to $\Delta A > 0$ and $\Delta A < 0$ respectively (b) Similar quantity, calculated with Eq.(5.34). Bottom panels: Scheme of the bijonction in different configurations: in (1), the dot level is resonant with the Fermi level of the normal metal, in (2), the dot level is resonant with a BCS peak of the superconductor, and in (3), the dot level has an energy higher than a BCS peak by ω_0, which enables inelastic tunneling with the emission of a photon.

sketched in panel 2. The blue area between these two types of resonances correspond to the photon emission area, where one has inelastic tunneling between the BCS peaks and the dot level, as sketched in panel 3. We could reproduce theoretically these data by calculating the charge susceptibility of the dot with a Keldysh Green's function formalism which takes into account tunneling to the fermionic reservoirs. More precisely, the charge susceptibility of the dot can be expressed as[72]

$$\Xi(\omega_0) = -iTr[\int \frac{d\omega}{2\pi} \mathcal{C}(\omega)\mathcal{G}^r(\omega)\Sigma^<(\omega)\left(\mathcal{G}^r(\omega)\right)^\dagger] \tag{5.34}$$

with

$$\mathcal{C}(\omega) = \hat{T}\left(\mathcal{G}^r(\omega+\omega_{RF}) + \mathcal{G}^r(\omega-\omega_{RF})^\dagger\right)\hat{T} \tag{5.35}$$

Above, $\mathcal{G}^r(\omega)$ is the retarded Greens' function of the dot, which depends on the tunnel rates between the dot and the reservoirs. This Greens' function has a 2*2 matrix structure (I will not give details here for brevity), in order to take into account the coupling between electron and hole excitations in a superconducting circuit. The lesser self energy $\Sigma^<(\omega)$ takes into account the filling of the reservoir levels, represented in the panels 1, 2 and 3 of Fig.5.5. The matrix $\hat{T} = diag(g_d, -g_d)$ accounts for the fact the energy of electrons and holes in the dot are shifted by $\pm g_d(\hat{a}^\dagger + \hat{a})$, accordingly with

Eq.(5.19). Equation (5.34) gives the theoretical result in Fig. 5.5b. The agreement between the data is quantitative, as shown by the use of the common colorscale for panels a and b.

It is interesting to note that the charge susceptibility expression of Eq.(5.34) is in fact valid for many geometries in the linear response regime. For instance, it can be generalized straightforwardly to the case where non-colinearly magnetized ferromagnetic contacts are used, or to the case of a multi quantum dot circuit, by using the relevant structure for the Green's function $\mathcal{G}^r$ and the self-energy $\Sigma^<(\omega)$. In the case of a device with several quantum dots, Eq.(5.34) enables one to recover dot-dot transitions described by equations similar to Eq.(5.33), on top of transitions between quantum dots and fermionic reservoirs. This equation can thus have a broad range of applications. I give an example of this fact in the next section.

Note that it is also possible to obtain photon emission by coupling a double quantum dot with normal metal contacts to a microwave cavity. In this case, the transition between the bounding and antibonding states of the cavity can emit photons if the double dot is voltage biased[106, 107]. This effect can even lead to a lasing effect if the double dot/cavity coupling is large enough[108]. In this last case, the linear description of the cavity response in terms of the double dot charge susceptibility, which is shown in Eq.(5.20), breaks down since lasing is a strongly non-linear effect. In this case, the cavity and double dot state occupations have to be calculated self-consistently (see for instance Ref.[112]).

5.9 Majorana nanocircuits

Majorana quasiparticles are among the most intriguing fermionic excitations predicted in condensed matter physics[110]. By definition, the fermionic creation operator $\hat{m}^\dagger$ of a Majorana quasiparticle is self adjoint, i.e. $\hat{m}^\dagger = \hat{m}$. This property offers possibilities of non-abelian statistics[111] and topologically protected quantum computation[113] in condensed matter systems. It has been found that different types of hybrid electronic circuits could enclose Majorana quasiparticles. In particular, hybrid structures combining a semiconducting nanowire in contact with a superconductor raise a lot of attention[114, 115, 116, 117, 118, 119, 120]. It has been predicted that in some situations, a single pair of overlapping Majorana bound states $(\hat{m}_L, \hat{m}_R)$ could appear in a semiconducting nanowire with spin-orbit coupling. These bound states have a spatial overlap which can be switched off with an external magnetic field or a gate

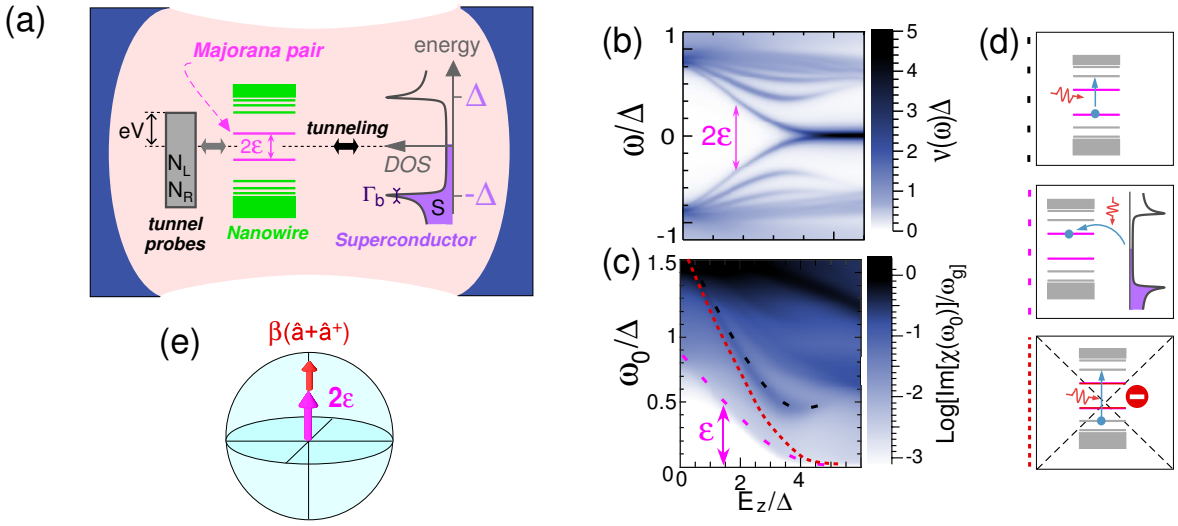

Fig. 5.6: (a) Energetic scheme of a Majorana nanowire coupled to a microwave cavity. The energy levels in the Majorana nanowire (green and pink lines) are coupled to a superconducting contact and two normal metal contacts. The Majorana doublet in pink has an energy splitting 2ε (b) Calculated density of states in the nanowire (c) Calculated microwave response of the cavity coupled to the nanowire (d) Schemes of the processes contributing to the resonances highlighted with the dashed lines in panel (c) (see main text) (e) Bloch schere representation of the device in the subspace of the Majorana pair. The fields corresponding to the Majorana free Hamiltonian in magenta and the coupling to the cavity in red are colinear.

voltage, in order to obtain two isolated Majorana bound states at zero energy[121, 122]. Recently, pairs of conductance peaks, with an energy splitting 2ε which oscillates and decays with the magnetic field, were observed, in striking agreement with these predictions[118, 119]. However, so far, mainly dc conductance measurements have been used, which reveal essentially the DOS of the nanowire[114, 115, 116, 117, 118, 119, 120]. This gives only a very indirect access to the property $\hat{m}^{\dagger}_{L(R)} = \hat{m}_{L(R)}$. A microwave cavity could represent an interesting tool to test more directly this property since the self-adjoint property $\hat{m}^{\dagger}_{L(R)} = \hat{m}_{L(R)}$ affects the structure of the light-matter coupling. We have considered theoretically this possibility during the Phd thesis of Matthieu Dartiailh (see Ref.[109]). More precisely, we have calculated the microwave response of a cavity coupled to a spin-orbit nanowire with a superconducting contact and two normal metal tunnel probes (Figure 5.6a). In practice, it is possible to measure simultaneously the cavity linewidth shift $\Delta\Lambda_0$, and the DOS of the nanowire by using the tunnel probes. We have used the Keldysh theory to calculate these two quantities, and in particular Eq.(5.34) to calculate $\Delta\Lambda_0$, by using a coarse grained description of

the nanowire into discrete sites. This requires to use a Green's function $\mathcal{G}^r(\omega)$ similar to that of section 5.8, with an extra-dimension corresponding to the site index. This leads to the results of Figures 5.6b and c, which I discuss below.

In the simplest situation, when a nanowire portion is driven to its topological phase, two Majorana bound states appear at the ends of the nanowire portion. The coupling 2ε between the two Majorana bound states tends to zero when the magnetic field increases, because this reduces their spatial overlap. As a result, one obtains in the DOS of the nanowire a pair of resonances at ε and $-\varepsilon$, which merge at zero energy ($\varepsilon = E_F$) for high magnetic fields, when the Majorana states do not overlap anymore (see Figure 5.6b). For an ordinary pair of fermionic states, one would generally get a cavity resonance for $\omega_0 = 2\varepsilon$, along the red dotted line in Fig.5.6c. However, no transition is visible in the calculated cavity signals at $\omega_0 = 2\varepsilon$. This can be understood by considering the fermionic anticommutation rule $\{\hat{m}^\dagger_{L(R)}, \hat{m}_{L(R)}\} = 1$ together with the self adjoint property $\hat{m}^\dagger_{L(R)} = \hat{m}_{L(R)}$, which give $\hat{m}_L^2 = 1$ and $\hat{m}_R^2 = 1$. This means that in the Majorana subspace, the nanowire unperturbed Hamiltonian and the coupling to the cavity have necessarily the same structure, i.e.

$$\hat{H}_0 = 2i\varepsilon\hat{m}_L\hat{m}_R \tag{5.36}$$

$$\hat{h}_{int} = 2i\beta\hat{m}_L\hat{m}_R \tag{5.37}$$

The β coefficient depends on the overlap of the two Majorana wavefunctions, since it corresponds to the type of coupling elements shown in Eq.(5.18). In a Bloch sphere representation, the vectors corresponding to the two above Hamiltonian components are colinear (see Figure 5.6e). This has to be compared with the case of the double dot (Fig.5.3c) where a transverse light/matter coupling exists. In the present case, since $[\hat{H}_0, \hat{h}_{int}] = 0$ in the Majorana subspace, the transition inside the Majorana pair is coupled only longitudinally to the cavity photons (no transverse coupling). This is why the transition inside the Majorana subspace at $\omega_0 = 2\varepsilon$ cannot exist in the cavity microwave response. Importantly, one should check experimentally that this selection rule is robust to changes in the system parameters like the applied magnetic field or the nanowire gate voltage, since it arises only from the fundamental property $\hat{m}^\dagger_{L(R)} = \hat{m}_{L(R)}$. One has to involve other system states to observe the Majorana pair with the microwave cavity. In particular, if one takes into account the fermionic states in the normal metal probes contacted to the nanowire, or a residual zero energy DOS in the superconductor, a step occurs in the $\Delta\Lambda_0$ signal at $\omega_0 = \varepsilon$, along the magenta

dashed line in Fig.5.6c. This feature is due to photo-assisted tunneling between the Majorana pair and the residual zero-energy DOS in the imperfect superconducting reservoir. Its visibility depends on the value of the coefficient β in Eq.(5.37), which has to be finite. This effect can be used to check that the low-energy doublet is well coupled to cavity photons, i.e. $\beta \neq 0$ in Eq.(5.37). Then, the simultaneous presence[absence] of the step at $\omega_0 = \varepsilon[2\varepsilon]$ would represent a good indication that the low energy doublet of Fig.5.6b indeed corresponds to self-adjoint states.

5.10 The Cooper pair splitter

The spatial separation of spin-entangled electrons of a Cooper pair extracted from a superconductor is an interesting goal in the context of quantum computation and communication[123, 124, 125, 126, 127]. In principle, a Cooper pair beam splitter (CPS) based on a double quantum dot connected to a central superconducting contact and two outer normal metal (N) contacts could facilitate this process[128] (see Fig.5.7). The spatial splitting of Cooper pairs has been demonstrated experimentally from an analysis of the CPS average currents, current noise, and current cross-correlations, in devices made out of a carbon nanotube[129, 130, 131, 132, 133, 134] or a semiconducting InAs quantum wire[135]. However, new tools appear to be necessary to investigate further the Cooper pair splitting dynamics, and in particular its coherence, which has not been demonstrated experimentally so far in the N/dot/S/dot/N geometry. This coherence has two intimately related aspects: the coherence of Cooper pair injection and the conservation of spin entanglement. The first aspect is due to the fact that Cooper pair injection into the CPS is a crossed Andreev process, which produces a coherent coupling between the initial and final states of the Cooper pair in the superconducting contact and the double dot (see for instances Refs.[136, 137]). In this context, coupling the CPS to a microwave cavity would be very interesting because it would enable one to perform the spectroscopy of the CPS and identify anticrossings in the CPS spectrum, which are due to the coherence of the injection process[138]. Detecting the conservation of spin entanglement represents an even greater challenge. In principle, in the presence of a real or artificial spin-orbit coupling, microwaves can produce transitions between the spin singlet and spin triplet states of the CPS, which reveal interferences due to the coherent superposition of spins states in the singlet. Therefore, a microwave cavity could represent an interesting tool to test the spin entanglement of split Cooper pairs[139].

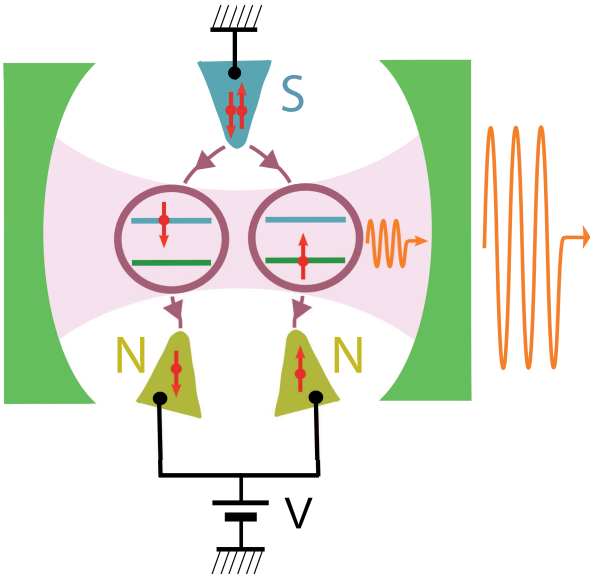

Fig. 5.7: Scheme of the Cooper pair splitter embedded in a microwave cavity. The Cooper pair splitter is made out of a double quantum dot (circles) coupled to a central blue superconducting contact (S) connected to ground, and two outer yellow normal metal contacts (N) biased with a voltage V. This circuit is placed inside a photonic cavity. The Cooper pairs spread over the orbitals of the dots, sketched in blue and green. The low energy level structure of the system allows photon emission which can be amplified by using for instance a lasing effect obtained for a finite V.

6. CONCLUSION AND PERSPECTIVES

Combining materials with different dimensionalities or electronic orders is interesting to obtain new phenomena. In this report, I have thus discussed the behavior of different hybrid quantum circuits. In chapter 3, I have discussed the case of metallic superconducting/ferromagnetic hybrid circuits, in which exotic superconducting correlations can be obtained. In chapter 4, I have discussed the case of hybrid nanocircuits which combine carbon nanotubes and ferromagnetic contacts. In this case, quantum interferences in the carbon nanotube enable one to control electrically spin transport. The hybridization of the quantum circuits can be pushed further by coupling them to a microwave cavity. In the resulting Mesoscopic QED devices, electrons of the quantum circuits are hybridized with cavity photons. As shown in chapter 5, this provides a powerful tool to investigate the electronic properties and dynamics of hybrid nanocircuits. In the semiclassical linear-coupling regime, a microwave cavity gives a direct access to the charge susceptibility of the nanocircuit. This picture is sufficient to interpret most of the experiment which have been performed so far. However, reaching the few photons quantum regime is also very interesting. This can be envisioned thanks to the different types of electronic degrees of freedom which have already been coupled coherently or strongly to cavity photons. In particular, recent experiments involve the charge[83, 84, 85] or spin[74] of a double dot. This should offer the opportunity to perform experiments similar to those performed in Cavity or Circuit QED, with new degrees of freedom. It is also possible to go beyond the paradigm of a two level system coupled to a cavity mode, if the tunneling dynamics of electrons to dissipative reservoirs is involved. This is well illustrated by photon emission effects triggered by out-of equilibrium electronic transport in a quantum dot circuit[72, 106, 107, 108]. Microwave cavities also represent an interesting tool to study exotic electronic condensed matter states such as split Cooper pairs[139, 138] or Majorana bound states[109]. Another possibility not discussed in this report is the study of the Kondo effect in quantum dots. I have recently collaborated with the HQC group to show that a microwave cavity can be used to observe the freezing of the charge dynamics in a Kondo dot[78].

Mesoscopic QED offers many more possibilities. This is why I intend to pursue my efforts for the development of this field in the next years...

BIBLIOGRAPHY

[1] A hysteretic single Cooper pair transistor for single-shot reading of a charge-qubit, A. Cottet, D. Vion, P. Joyez, D. Esteve, and M.H. Devoret, p. 73 in "International Workshop on Superconducting Nano-electronics Devices " J. Pekola, B. Ruggiero, and P. Silvestrini eds., Kluwer Academic, Plenum Publishers, New York (2002).

[2] Superconducting electrometer for measuring the single Cooper pair box, A. Cottet, A. Steinbach, P. Joyez, D.Vion, H. Pothier, and D. Esteve, M.E. Huber, pp. 111 in: "Macroscopic Quantum Coherence and Quantum Computing", D.V. Averin, B. Ruggiero, P. Silvestrini eds., Kluwer Academic, Plenum Publishers, New York (2001).

[3] A. Cottet, D. Vion, P. Joyez, A. Aassime, D. Esteve, and M.H. Devoret, 2002 *Physica C* **367**, 197

[4] D. Vion, A. Aassime, A. Cottet, P. Joyez, H. Pothier, C. Urbina, D. Esteve, and M.H. Devoret, 2002, *Science* **296**, 886

[5] Albert Fert, Rev. Mod. Phys. 80, 1517 (2008)

[6] J. Medford, J. Beil, J. M. Taylor, E. I. Rashba, H. Lu, A. C. Gossard, and C. M. Marcus 2013 *Phys. Rev. Lett.* **111** 050501

[7] Hanbury Brown R and Twiss R Q (1956) *Nature* **178** 1046

[8] M. Büttiker, Phys. Rev. B 46, 12 485 (1992).

[9] M. Henny, S. Oberholzer, C. Strunk, T. Heinzel, K. Ensslin, M.Holland, and C. Schönenberger, Science 284, 296 (1999)

[10] W. D. Oliver, J. Kim, R. C. Liu, and Y. Yamamoto, Science 284, 299 (1999)

[11] A. Cottet, W. Belzig, and C. Bruder 2004 *Phys. Rev. Lett.* **92**, 206801

[12] A. Cottet, W. Belzig, and C. Bruder 2004 *Phys. Rev. B* **70**, 115315 (2004).

[13] Y. Zhang et al. 2007 *Phys. Rev. Lett.* **99**, 036603 (2007)

[14] A. Cottet 2007 *Phys. Rev. B* **76**, 224505

[15] A. Cottet and W. Belzig 2005 *Phys. Rev. B* **72**, 180503(R)

[16] Buzdin A I 2005 Rev. Mod. Phys. **77**, 935

[17] Fulde P and Ferrell R A 1964 *Phys. Rev.* **135** A550

[18] T. Kontos, M. Aprili, J. Lesueur, and X. Grison 2001 *Phys. Rev. Lett.* **86**, 304

[19] Kontos et al. 2002 *Phys. Rev. Lett.* **89**, 137007

[20] A. Cottet and W. Belzig 2008 *Phys. Rev. B* **77**, 064517

[21] A. Cottet, B. Douçot and W. Belzig 2008 *Phys. Rev. Lett.* **101**, 257001 (2008).

[22] Cottet A, Kontos T, Belzig W, Schönenberger C and Bruder C 2006 *Europhys. Lett.* **74** 320

[23] A. Cottet and M.-S. Choi 2006 *Phys. Rev. B.* **74**, 235316

[24] Meir et al. 1991 *Phys. Rev. Lett.* **66**, 3048

[25] S. Sahoo, T. Kontos, J. Furer, C. Hoffmann, M. Graber, A. Cottet and C. Schönenberger 2005 *Nature Phys.* 1, **99**

[26] Martinek, J. et al. 2005 Phys. Rev. B **72**, 121302

[27] Sindel M. et al. 2007 *Phys. Rev. B* **76**, 45321

[28] S. Koller, J. Paaske, M. Grifoni 2012 *Phys. Rev. B* **85**, 045313

[29] Dirnaichner A, Grifoni M, Prüfling A, Steininger D, Hüttel A K and Strunk C 2015 *Phys. Rev. B* **91**, 195402

[30] K.D. Usadel 1970, *Phys. Rev. Lett.* **25**, 507

[31] Huertas-Hernando D, Nazarov Yu V and Belzig W 2002 Phys. Rev.Lett. 88, 047003.

[32] Huertas-Hernando D and Nazarov Yu V 2005 Eur. Phys. J. B 44, 373.

[33] Cottet A 2007 Phys. Rev. B 76 224505

[34] Cottet A and J. Linder 2009 Phys. Rev. B 79, 054518 .

[35] Cottet A and Belzig W 2005 Phys. Rev. B 72, 180503 R .

[36] Linder J, Yokoyama T, and Sudbø A 2009 Phys. Rev. B 79, 054523.

[37] Morten J P, Huertas-Hernando D, Brataas A, and Belzig W 2008 EPL 81, 40002 .

[38] Morten J P, Huertas-Hernando D, Belzig W, and Brataas A 2008 Phys. Rev. B 78, 224515.

[39] Braude V and Nazarov Yu V 2007 Phys. Rev. Lett. 98, 077003.

[40] Linder J, Yokoyama T, Sudbø A, and Eschrig M 2009 Phys. Rev. Lett. 102, 107008

[41] Di Lorenzo A and Nazarov Yu V 2005 Phys. Rev. Lett. 94, 210601

[42] M.Yu. Kuprianov and V.F. Lukichev 1988 *Sov. Phys. JETP* **67** 1163

[43] A. Cottet, D. Huertas-Hernando, W. Belzig, and Y. V. Nazarov 2009 *Phys. Rev. B* **80**, 184511

[44] M. Eschrig, A. Cottet, W. Belzig, J. Linder 2015 *New J. Phys.* **17** 083037

[45] V. V. Ryazanov, V. A. Oboznov, A. Yu. Rusanov, A. V. Veretennikov, A. A. Golubov, and J. Aarts 2001 *Phys. Rev. Lett.* **86** 2427

[46] R. S. Keizer1, S. T. B. Goennenwein, T. M. Klapwijk, G. Miao, G. Xiao and A. Gupta 2006 *Nature* **439**, 825

[47] Khaire T S et al, *Phys. Rev. Lett.***104**, 137002 (2010)

[48] Robinson JW A et al., *Science* **329**, 59 (2010)

[49] Sprungmann D et al., *Phys. Rev. B* **82**, 060505 (2010)

[50] Datta,S and Das B 1990 *Applied Physics Letters* **56** 665

[51] A. Cottet 2011 *Phys. Rev. Lett.* **107**, 177001

[52] A. Cottet, C. Feuillet-Palma, and T. Kontos 2009 *Phys. Rev. B* **79**, 125422

[53] C. Feuillet-Palma, T. Delattre, P. Morfin, J.-M. Berroir, G. Fève, D.C. Glattli, B. Plaçais, A. Cottet and T. Kontos 2010 *Phys. Rev. B* **81**, 115414

[54] A.D. Crisan, S. Datta, J.J. Viennot, M.R. Delbecq, A.Cottet and T.Kontos 2016 *Nature Communications* **7**, Article number: 10451

[55] Raimond J M, Brune M and Haroche S 2001 *Rev. Mod. Phys.* **73**, 565

[56] Wallraff A, Schuster D I, Blais A, Frunzio L, Huang R, Majer J, Kumar S, Girvin S M, Schoelkopf R J, 2004 *Nature* **431**, 162

[57] Childress L, Sørensen A S and Lukin M D 2004 *Phys. Rev. A* **69** 042302.

[58] Delbecq M R, Schmitt V, Parmentier F D, Roch N, Viennot J J , Fève G, Huard B, Mora C, Cottet A and Kontos T 2011 *Phys. Rev. Lett.* **107** 256804

[59] J. P. Reithmaier, G. Sek, A. Löffler, C. Hofmann, S. Kuhn, S. Reitzenstein, L. V. Keldysh, V. D. Kulakovskii, T. L. Reinecke, A. Forchel 2004 Nature 432, 197

[60] T. Yoshie, A. Scherer, J. Hendrickson, G. Khitrova, H. M. Gibbs, G. Rupper, C. Ell, O.B. Shchekin, D. G. Deppe 2004 Nature 432, 200

[61] Frey T, Leek P J, Beck M, Ensslin K, Wallraff A and Ihn T 2011 *Appl. Phys. Lett.* **98** 262105

[62] Toida H, Nakajima T and Komiyama S 2012 *Phys. Rev. Lett.* **110** 066802

[63] Schmidt A R, Henry E, Lo C C, Wang Y T, Li H, Greenman L, Namaan O, Schenkel T, Whaley K B, Bokor J, Yablonovitch E and Siddiqi I 2014 *J. Appl. Phys.* **116** 044503

[64] X. Mi, J. V. Cady, D. M. Zajac, J. Stehlik, L. F. Edge, J. R. Petta 2017 *Appl. Phys. Lett.* **110** 043502

[65] Ranjan V, Puebla-Hellmann G, Jung M, Hasler T, Nunnenkamp A, Muoth M, Hierold, Wallraff C and Schönenberger 2015 *Nature Communications* **6** 7165

[66] Petersson K D, McFaul L W, Schroer M D, Jung M, Taylor J M, Houck A A and Petta J R 2012 *Nature* **490**, 380

[67] Larsen T W, Petersson K D, Kuemmeth F, Jespersen T S, Krogstrup P, Nygard J and Marcus C M 2015 *Phys. Rev. Lett.* **115**, 127001

[68] de Lange G, van Heck B, Bruno A, van Woerkom D J, Geresdi A, Plissard S R, Bakkers E P A M, Akhmerov A R and DiCarlo L 2015 *Phys. Rev. Lett.* **115**, 127002

[69] Wang R, Deacon R S, Car D, Bakkers E P A M and Ishibashi K 2016 *Appl. Phys. Lett.* **108** 203502

[70] Zhang M-L, Wei D, Deng G-W, Li S-X, Li H-O, Cao G, Tu T, Xiao M, Guo G-C, Jiang H-W and Guo G-P 2014 *Appl. Phys. Lett.* **105** 073510

[71] Janvier C, Tosi L, Bretheau L, Girit Ç Ö, Stern M, Bertet P, Joyez P, Vion D, Esteve D, Goffman M F, Pothier H and Urbina C 2015 *Science* **349** 1199

[72] Bruhat L E, Viennot J J, Dartiailh M C, Desjardins M M, Kontos T and Cottet A 2016 *Phys. Rev. X* **6** 021014

[73] Cottet A, Kontos T, Sahoo S, Man H T, Choi M-S, Belzig W, Bruder C, Morpurgo A F and Schönenberger C 2006 *Semicond. Sci. Technol.* **21** S78

[74] Viennot J J, Dartiailh M C, Cottet A and Kontos T 2015 *Science* **349** 408

[75] Cottet A, Kontos T and Douçot B 2015 *Phys. Rev. B* **91**, 205417

[76] Cohen-Tannoudji C, Dupont-Roc J, and Grynberg G 1997 *Photons and Atoms: Introduction to Quantum Electrodynamics* (New York: Wiley)

[77] Prange R E 1963 *Phys. Rev.* **131**, 1083

[78] Desjardins M M, Viennot J J, Dartiailh M C, Bruhat L E, Delbecq M R, Lee M, Choi M-S, Cottet A and Kontos T 2017 *Nature* **545**, 71

[79] Frey T, Leek P J, Beck M, Blais A, Ihn T, Ensslin K and Wallraff A 2012 *Phys. Rev. Lett.* **108** 046807

[80] Blais A, Huang R-S, Wallraff A, Girvin S M and Schoelkopf R J 2004 *Phys. Rev.A* **69**, 062320

[81] Schroer M D, Jung M, Petersson K D and Petta J R 2012 *Phys. Rev. Lett.* **109** 166804

[82] Frey T, Leek P J, Beck M, Faist J, Wallraff A, Ensslin K, Ihn T and Büttiker M 2012 *Phys. Rev. B* **86** 115303

[83] Mi X, Cady J V, Zajac D M, Stehlik J, Edge L F and Petta J R 2017 *Science* **355** 156

[84] Bruhat L E, Cubaynes T, Viennot J J, Dartiailh M C, Desjardins M M, Cottet A and Kontos T, arXiv:1612.05214

[85] Stockklauser A, Scarlino P, Koski J, Gasparinetti S, Kraglund Andersen C, Reichl C, Wegscheider W, Ihn T, Ensslin K, Wallraff A arXiv:1701.03433

[86] Cottet A and Kontos T 2010 *Phys. Rev. Lett.* **105** 160502

[87] Viennot J J, Delbecq M R, Dartiailh M C, Cottet A and Kontos T 2014 *Phys. Rev. B* **89** 165404

[88] Pályi A and Burkard G, 2011 *Phys. Rev. Lett.* **106**, 086801

[89] Pályi A and Burkard G 2010 *Phys. Rev. B* **82**, 155424

[90] Burkard G and Petta J R 2016 *Phys. Rev. B* **94**, 195305

[91] Hornberger R P, Koller S, Begemann G, Donarini A and Grifoni M 2008 *Phys. Rev. B* **77**, 245313

[92] Trif M, Golovach V N and Loss D 2008 *Phys. Rev. B* **77** 045434

[93] Xuedong H, Yu-xi L and Franco N 2012 *Phys. Rev. B* **86** 035314

[94] Kloeffel C, Trif M, Stano P and Loss D 2013 *Phys. Rev. B* **88** 241405(R)

[95] Salfi J, Mol J A, Culcer D and Rogge S 2016 *Phys. Rev. Lett.* **116** 246801

[96] Beaudoin F, Lachance-Quirion D, Coish W A and Pioro-Ladrière M 2016 *Nanotechnology* **27**, 464003

[97] Burkard G and Imamoglu A 2006 *Phys. Rev. B* **74** 041307(R)

[98] Pei-Qing J, Marthaler M, Shnirman A and Schön G 2012 *Phys. Rev. Lett.* **108** 190506

[99] Pei-Qing J, Jeske J, Greentree A D and Cole J H arXiv:1507.07198

[100] Wang L, Tu T, Gong B and Guo G-C 2015 *Phys. Rev. A* **92** 062346

[101] Tian-Yi H; Guang-Wei D, Wei D and Guo-Ping G 2016 *Chinese Physics Letters* **33**4

[102] Russ M and Burkard G 2015 *Phys. Rev. B* **92** 205412

[103] Srinivasa V, Taylor J M and Tahan C 2016 *Phys. Rev. B* **94** 205421

[104] Russ M, Ginzel F and Burkard G 2016 *Phys. Rev. B* **94** 165411

[105] Arnold C, Demory J, Loo V, Lemaître A, Sagnes I, Glazov M, Krebs O, Voisin P, Senellart P and Lanco L 2015 *Nature Comm.* **6** Article number: 6236

[106] Stockklauser A, Maisi V F, Basset J, Cujia K, Reichl C, Wegscheider W, Ihn T, Wallraff A and Ensslin K 2015 *Phys. Rev. Lett.* **115** 046802

[107] Liu Y Y, Petersson K D, Stehlik J, Taylor J M and Petta J R 2014 *Phys. Rev. Lett.* **113** 036801

[108] Liu Y-Y, Stehlik J, Eichler C, Gullans M J, Taylor J M and Petta J R 2015 *Science* **347** 285

[109] Dartiailh M, Kontos T, Douçot M and Cottet A, Phys. Rev. Lett. 2017 (in press) and ArXiv: 1702.01637

[110] Kitaev A Y 2001 *Phys.Usp.* **44**, 131

[111] D. A. Ivanov Phys. Rev. Lett. **86**, 268 (2001).

[112] André S, Brosco V, Marthaler M, Shnirman A, and Schön G 2009 Phys. Scr.**T137**, 014016

[113] Nayak C, Simon S H, Stern A, Freedman M and Das Sarma S 2008 *Rev. Mod. Phys.* **80**, 1083

[114] Mourik V, Zuo K, Frolov S M, Plissard S R, Bakkers E P A M, and Kouwenhoven L P 2012 *Science* **336**, 1003

[115] Das A, Ronen Y, Most Y, Oreg Y, Heiblum M and Shtrikman 2012 *Nat. Phys.* **8**, 887

[116] Deng M T, Yu C L, Huang G Y, Larsson M, Caroff P, and Xu H Q 2012 Nano Letters **12**, 6414

[117] Churchill H O H, Fatemi V, Grove-Rasmussen K, Deng M T, Caroff P, Xu H Q and Marcus C M 2013 *Phys. Rev. B* **87**, 241401

[118] Albrecht S M, Higginbotham A P, Madsen M,Kuemmeth F, Jespersen T S, Nygård J, Krogstrup P and Marcus C M Nature **531**, 206 (2016).

[119] Deng M T, Vaitiekenas S, Hansen E B, Danon J., Leijnse M, Flensberg K, Nygård J, Krogstrup P and Marcus C M *Science* **354** 1557 (2016)

[120] Zhang H et al., arXiv:1603.04069

[121] Lutchyn R M, Sau J D and Das Sarma S 2010 *Phys. Rev. Lett.* **105**, 077001

[122] Oreg Y, Refael G, and von Oppen F 2010 *Phys. Rev. Lett.* **105**, 177002

[123] T. Martin 1996 *Phys. Lett. A* **220**, 137

[124] M. P. Anantram and S. Datta 1996 *Phys. Rev. B* **53** 16390

[125] G. Burkard, D. Loss, and E. V. Sukhorukov 2000 *Phys. Rev. B* **61**, R16303 (2000)

[126] S. Kawabata 2001 *J. Phys. Soc. Jpn.* **70**,1210

[127] G. B. Lesovik, T. Martin,and G. Blatter 2001 *Eur. Phys. J. B* **24**, 287

[128] Recher P, Sukhorukov E V, and Loss D 2001 *Phys. Rev. B* **63** 165314

[129] Hofstetter L, Csonka S, Nygård J and Schönenberger C *Nature* **461**, 960 (2009)

[130] Herrmann L G, Portier F, Roche P, Levy Yeyati A, Kontos T, and Strunk C, 2010 *Phys. Rev. Lett.* **104**, 026801 (2010)

[131] Hofstetter L, Csonka S, Baumgartner A, Fülöp G, d'Hollosy S, Nygård J and Schönenberger C, Phys. Rev. Lett. **107**, 136801 (2011)

[132] Schindele J, Baumgartner A and Schönenberger C 2012 *Phys. Rev. Lett.* **109**, 157002

[133] Herrmann L G, Burset P, Herrera W J, Portier F, Roche P, Strunk C, Levy Yeyati A, and Kontos T, arXiv:1205.1972

[134] Schindele J, Baumgartner A, Maurand R, Weiss M, and Schönenberger C, Phys. Rev. B, **89**, 045422 (2014).

[135] Das A, Ronen Y, Heiblum M, Mahalu D, Kretinin A V and Shtrikman H, 2012 *Nature Comm.* **3**, Article number: 1165

[136] O. Sauret, D. Feinberg, and T. Martin 2004 *Phys. Rev. B* **70**, 245313

[137] J. Eldridge, M. G. Pala, M. Governale, and J. König 2010 *Phys. Rev. B* **82**,184507

[138] Cottet A 2014 *Phys. Rev. B* **90** 125139

[139] Cottet A, Kontos T and Levy Yeyati A 2012 *Phys. Rev. Lett.* **108** 166803

[140] Kirchmair et al. 2013 *Nature* **495**, 205

[141] Sarlette et al. 2011 *Phys. Rev. Lett.* **107**, 010402

[142] Leghtas et al, *Science* **347**, 6224 (2015)